NASA/TM—2016-218946/REV1

Hardness and Microstructure of Binary and Ternary Nitinol Compounds

Malcolm K. Stanford
Glenn Research Center, Cleveland, Ohio

This Revised Copy, numbered as NASA/TM—2016-218946/REV1, December 2019, supersedes the previous version, NASA/TM—2016-218946, January 2016, in its entirety.

December 2019

NASA STI Program . . . in Profile

Since its founding, NASA has been dedicated to the advancement of aeronautics and space science. The NASA Scientific and Technical Information (STI) Program plays a key part in helping NASA maintain this important role.

The NASA STI Program operates under the auspices of the Agency Chief Information Officer. It collects, organizes, provides for archiving, and disseminates NASA's STI. The NASA STI Program provides access to the NASA Technical Report Server—Registered (NTRS Reg) and NASA Technical Report Server—Public (NTRS) thus providing one of the largest collections of aeronautical and space science STI in the world. Results are published in both non-NASA channels and by NASA in the NASA STI Report Series, which includes the following report types:

- TECHNICAL PUBLICATION. Reports of completed research or a major significant phase of research that present the results of NASA programs and include extensive data or theoretical analysis. Includes compilations of significant scientific and technical data and information deemed to be of continuing reference value. NASA counter-part of peer-reviewed formal professional papers, but has less stringent limitations on manuscript length and extent of graphic presentations.

- TECHNICAL MEMORANDUM. Scientific and technical findings that are preliminary or of specialized interest, e.g., "quick-release" reports, working papers, and bibliographies that contain minimal annotation. Does not contain extensive analysis.

- CONTRACTOR REPORT. Scientific and technical findings by NASA-sponsored contractors and grantees.

- CONFERENCE PUBLICATION. Collected papers from scientific and technical conferences, symposia, seminars, or other meetings sponsored or co-sponsored by NASA.

- SPECIAL PUBLICATION. Scientific, technical, or historical information from NASA programs, projects, and missions, often concerned with subjects having substantial public interest.

- TECHNICAL TRANSLATION. English-language translations of foreign scientific and technical material pertinent to NASA's mission.

For more information about the NASA STI program, see the following:

- Access the NASA STI program home page at http://www.sti.nasa.gov

- E-mail your question to help@sti.nasa.gov

- Fax your question to the NASA STI Information Desk at 757-864-6500

- Telephone the NASA STI Information Desk at 757-864-9658

- Write to:
  NASA STI Program
  Mail Stop 148
  NASA Langley Research Center
  Hampton, VA 23681-2199

NASA/TM—2016-218946/REV1

Hardness and Microstructure of Binary and Ternary Nitinol Compounds

Malcolm K. Stanford
Glenn Research Center, Cleveland, Ohio

This Revised Copy, numbered as NASA/TM—2016-218946/REV1, December 2019, supersedes the previous version, NASA/TM—2016-218946, January 2016, in its entirety.

National Aeronautics and
Space Administration

Glenn Research Center
Cleveland, Ohio 44135

December 2019

Acknowledgments

A sincere thanks to Peter J. Bonacuse, Joy A. Buehler, Jesse R. Bierer, Ankesh Madan, Jordan D. McCrone, Dr. Quynhgiao N. Nguyen, Edward L. Pang, Dr. Richard B. Rogers, and Walter A. Wozniak for all of their technical assistance and to Drs. Othmane Benafan, Anita Garg and Ronald D. Noebe for numerous technical discussions. This work was funded by the NASA's Transformational Tools and Technologies Project.

Revised Copy

This Revised Copy, numbered as NASA/TM—2016-218946/REV1, December 2019, supersedes the previous version, NASA/TM—2016-218946, January 2016, in its entirety.

Additional etching was found to be necessary to reveal fine microstructural phases in Figure 7(b), Figures 11(a) to (c), Figure 15(c), Figure 16(b), and Figure 20(c). Based on this, it was also determined that light etching, in addition to that provided by the colloidal silica polishing medium, helped to enhance the contrast between the parent and precipitate phases. Therefore, additional second-phase measurements were made for alloys 52-3T, 53-3T, 54-3T, 54-3H, 54-3Z, 55-3T, 55-3H, and 55-3Z after heat treatment at 800 °C to improve measurement of statistical variation. For alloy 55-3H, second-phase measurements were performed at 500× magnification using a Normarski filter to enhance visual contrast and measurement accuracy. For Figure 37, the number of hardness measurements was doubled from 5 to 10 in an attempt to reduce the statistical variation within some of the alloys.

It was determined that in Figure 7(a), Figure 9(d), and Figure 11(d), incorrect images were presented due to typographical errors. The correct images now appear in these three figures. Additionally, some images were recaptured simply to match the contrast and brightness of the other images that were on the same page for better visual comparison.

Level of Review: This material has been technically reviewed by technical management.

Available from

NASA STI Program
Mail Stop 148
NASA Langley Research Center
Hampton, VA 23681-2199

National Technical Information Service
5285 Port Royal Road
Springfield, VA 22161
703-605-6000

This report is available in electronic form at http://www.sti.nasa.gov/ and http://ntrs.nasa.gov/

Hardness and Microstructure of Binary and Ternary Nitinol Compounds

Malcolm K. Stanford
National Aeronautics and Space Administration
Glenn Research Center
Cleveland, Ohio 44135

Abstract

The hardness and microstructure of twenty-six binary and ternary Nitinol compounds (Ni-Ti, Ni-Ti-Ta, Ni-Ti-Hf, and Ni-Ti-Zr) were studied. A small (50g) button of each compound was produced by vacuum arc melting (VAM). Each alloy was homogenized in vacuum for 48 hr followed by furnace cooling. Specimens from the buttons were then heat treated at 800, 900, 1000 or 1100 °C for 2 hr followed by water quenching. The hardness and microstructure of each specimen was compared to the baseline (55-Nitinol, 55 at.% Ni – 45 at.% Ti, after heat treatment at 900 °C). The results show that sixteen of the studied compounds had higher hardness values than the baseline material with relatively low levels of secondary phase precipitation. Moreover, five of these compounds had hardness values greater than or equal to approximately 660HV (≈58HRC) with essentially no property-degrading precipitation phases.

Background

The Ni-rich intermetallic nickel-titanium compound known as 60-Nitinol began being developed for engineering applications nearly 50 years ago but was shelved because it was difficult to machine to tight tolerances due to warping (Ref. 1). More recent work at NASA has shown that this material has great potential for aerospace bearing applications but dimensional distortion during processing has remained a recalcitrant issue (Refs. 2 to 4).

The heat treatment process required to harden 60-Nitinol to acceptable values for bearing applications requires the material to be heated above the solvus at approximately 1050 °C and then rapidly quenched (Ref. 5). This heat treatment, if above the solvus temperature, is designed to render the material single phase in its B2 cubic austenitic form. Due to the high concentration of Ni, however, a metastable Ni_4Ti_3 phase will precipitate during cooling (Ref. 6). This fine phase precipitation hardens the material. The goal of the rapid quench is primarily to prevent formation of the metastable Ni_3Ti_2 phase or the equilibrium Ni_3Ti phase. These phases do not induce hardening but actually lead to softening in the material by reducing the amount of metastable Ni_4Ti_3 phase present (Refs. 6 and 7). Even so, the high level of residual stress created in a part after undergoing the drastic heat treatment just described is the likely cause of the observed dimensional distortion with this material. The purpose of this investigation was to determine if the solvus temperature of Ni-rich nickel-titanium compounds could be reduced with certain ternary additions, thereby reducing the severity of the heat treatment and, the propensity for dimensional distortion. This determination will be made by measuring the hardness of the material and percentage of second phase present in the microstructure.

Experimental Procedures

Nickel and titanium pellets, tantalum powder and hafnium and zirconium chips were purchased from commercial sources. The purity of each material was certified by the supplier as listed in Table 1. Only the impurities at levels of 1 ppm or greater are reported. It should be noted that Zr typically accompanies Hf because they are found together in nature and are difficult to separate due to their chemical similarity (Refs. 8 and 9).

Twenty-six Ni-rich binary intermetallic Ni-Ti compounds and ternary Ni-Ti-Ta, Ni-Ti-Hf or Ni-Ti-Zr compounds (listed in Table 2) were produced by vacuum arc melting (Ref. 10). In this process, a water-cooled copper crucible was charged with the desired composition for each compound. The charge consisted of the requisite combination of the granular elemental materials on a weight basis. The melting chamber was sealed, evacuated with a mechanical pump to a pressure of approximately 10^{-3} torr, and then backfilled with argon to a partial pressure of approximately 500 torr (~2/3 atm). A tungsten electrode was used to strike an arc with the copper crucible, heating the charge to a molten state. To increase chemical homogeneity, each button was allowed to cool and then inverted in the crucible before being remelted. This process was repeated a total of five times, resulting in a small button weighing approximately 50g, as shown in Figure 1. The buttons were homogenized at 1050 °C for 48 in vacuum (approximately 10^{-6} torr) followed by furnace cooling and then sectioned by wire electrical discharge machining into 5 mm cubic specimens. The chemical compositions of the studied compounds (see Table 2) were analyzed by inductively-coupled plasma atomic emission spectroscopy (ICP-AES).

To study the effect of heat treatment temperature on microstructure and hardness, each specimen was heat treated for 2 hr at 800, 900 or 1,000 °C in vacuum. The binary compounds and the compounds containing 1 or 5 at.% Hf were also heat treated at 1,100 °C (also in vacuum). The furnace chamber was rapidly backfilled with argon so that the specimens could be drop-quenched in water. The heat treated specimens were mounted in Bakelite and prepared for microscopy with standard metallographic techniques, including a final polish using colloidal silica on a vibratory polisher. This procedure produced a high-quality surface finish for microscopic examination. For the binary compounds, it was discovered that the slight alkalinity of the colloidal silica solution used in the final polish provided a mild etch that enhanced the contrast between the medium grey B2 parent phase and the light grey precipitate phases. The precipitate phases consisted of Ni_3Ti, which had a globular morphology, and Ni_3Ti_2, which had a plate- or needle-like morphology (Refs. 11 and 12). The Ni_4Ti_3 phase also has a plate- or needle-like morphology, but this phase was generally too fine to be resolved distinctly from the parent phase using this method. Therefore, the secondary phase measurements included only the noncoherent Ni_3Ti and Ni_3Ti_2 phases, which tend to reduce hardening.

TABLE 1.—CHEMICAL COMPOSITION OF ELEMENTAL MATERIALS USED IN THIS STUDY

Element	Purity, percent	Major impurities, ppm
Ni	99.999	C (10), Co (1), Fe (12) N (1), O (5), S (2)
Ti	99.995	C (11), Fe (5), H (1), N(<10), Ni (1), O (216), Rb (<5), S (<5), Sr (<3000), Ta (<5), Y (<200)
Ta	99.98	Nb (50), O (1200), H (<20), C (30), N (30), Si (<30), Ti (5), Mo (5), W (<10). Ni (<20), Fe (20), Cr (<10), Mn (5),, Na (<10), K (<10), Nb (<30), Mg (5)
Hf	99.7	Al (<25), B (<0.5), Bi (<1), C (<20), Cd (<3), Cr (<30), Co (<5), Cu (<20), Fe (<50), H (<3), Mg (<10), N (<5), Nb (<50), Ni (<25), O (<53), P (<3), Pb (<5), S (<10), Si (<25), Sn (<10), Ta (<1), Th (<4), Ti (<20), U (<2), V (<10), W (<20), Zr (14000)
Zr	99.5	Al (<20), B (<0.25), C (<31), Cd (<0.25), Co (<10), Cr (<50), Cu (<25), Fe (<50), H (22), Hf (28), Mn (<25), Mo (<10), N (<20), Nb (<50), Ni (<35), O (80), P (5), Pb (<25), Si (<10), Sn (<35), Ta (<100), Ti (<25), U (<1), V (<25), W (<30)

TABLE 2.—COMPOSITIONS OF THE STUDIED INTERMETALLIC COMPOUNDS

Designation	Target composition, at.%	Ni, wt.% [at.%]	Ti, wt.% [at.%]	X, wt.% [at.%]	Impurities, ppm
51	Ni_{51}-Ti_{49}	56.2 [51.1]	43.8 [48.9]	N/A	Al (30), B (40), Ca (1), Fe (10), Mn (2), Mo (20), Si (40), C (120), N (15), O (230)
52	Ni_{52}-Ti_{48}	56.8 [51.8]	43.1 [48.2]	N/A	Al (10), Cu (40), Fe (10), Mo (30), C (80), N (<10), O (160)
53	Ni_{53}-Ti_{47}	57.7 [52.7]	42.2 [47.3]	N/A	Al (50), Cu (90), Fe (30), Mo (30), C (115), N (25), O (325)
54	Ni_{54}-Ti_{46}	58.3 [53.6]	41.1 [46.3]	N/A	Al (10), Cu (20), Fe (20), Mo (30), W (4800), C (80), N (10), O (230)
55	Ni_{55}-Ti_{45}	59.1 [54.2]	40.7 [45.8]	N/A	Al (10), Co (20), Cu (100), Fe (10), Mo (30), W (1300), C (80), N (<10), O (220)
56	Ni_{56}-Ti_{44}	60.4 [55.5]	39.5 [44.5]	N/A	Al (10), Co (20), Cu (80), Fe (20), Mo (30), W (200), C (75), N (10), O (210)
52-1H	Ni_{52}-Ti_{47}-Hf_1	55.4 [51.7]	41.3 [47.3]	3.25 Hf [1.00]	Al (20), Cu (60), Fe (20), Mo (20), Zr (400), C (60), N (35), O (205)
53-1H	Ni_{53}-Ti_{46}-Hf_1	56.8 [53.1]	40.0 [45.9]	3.15 Hf [0.97]	Al (20), Cu (70), Fe (10), Mo (20), Zr (400), C (60), N (<10), O (180)
54-1H	Ni_{54}-Ti_{45}-Hf_1	57.6 [54.4]	38.4 [44.4]	3.27 Hf [1.01]	Al (20), Co (40), Cu (700), Fe (10), Mo (20), W (5300), Zr (400), C (70), N (10), O (260)
55-1H	Ni_{55}-Ti_{44}-Hf_1	56.9 [53.3]	39.8 [45.7]	3.16 Hf [0.97]	Al (10), Cu (20), Fe (10), Mo (20), W (50), Zr (400), C (70), N (30), O (280)
52-3H	Ni_{52}-Ti_{45}-Hf_3	53.3 [52.5]	36.7 [44.3]	9.73 Hf [3.15]	Zr (1300), Cu (250), Fe (15), Mn (3), Mo (20), Si (140), C (70), N (3), O (410)
53-3H	Ni_{53}-Ti_{44}-Hf_3	54.4 [53.6]	35.9 [43.3]	9.46 Hf [3.06]	Zr (1300), Cu (330), Fe (15), Mn (3), Mo (20), Si (140), C (60), N (3), O (330)
54-3H	Ni_{54}-Ti_{43}-Hf_3	55.2 [54.6]	34.9 [42.3]	9.48 Hf [3.08]	Zr (1300), Cu (310), Fe (15), Mn (6), Mo (20), Si (980), C (60), N (2), O (310)
55-3H	Ni_{55}-Ti_{42}-Hf_3	56.0 [55.4]	34.1 [41.4]	9.61 Hf [3.13]	Zr (1300), Cu (50), Fe (15), Mn (6), Mo (20), Si (80), C (60), N (2), O (180)

Designation	Target composition, at.%	Ni, wt.% [at.%]	Ti, wt.% [at.%]	X, wt.% [at.%]	Impurities, ppm
52-3T	Ni_{52}-Ti_{45}-Hf_3	53.5 [52.7]	36.6 [44.2]	9.71 Ta [3.10]	Cu (400), Fe (35), Mn (4), Mo (20), Si (160), C (70), N (6), O (400)
53-3T	Ni_{53}-Ti_{44}-Hf_3	54.5 [53.7]	35.8 [43.2]	9.63 Ta [3.08]	Cu (290), Fe (35), Mn (5), Mo (20), Si (160), C (70), N (3), O (370)
54-3T	Ni_{54}-Ti_{43}-Hf_3	55.2 [54.5]	35.0 [42.4]	9.68 Ta [3.10]	Cu (80), Fe (35), Mn (7), Mo (20), Si (400), C (60), N (1), O (200)
55-3T	Ni_{55}-Ti_{42}-Hf_3	56.0 [55.5]	34.2 [41.4]	9.66 Ta [3.10]	Cu (10), Fe (35), Mn (8), Mo (20), Si (700), C (60), N (2), O (220)
52-3Z	Ni_{52}-Ti_{45}-Zr_3	56.2 [52.6]	38.5 [44.2]	5.22 Zr [3.15]	Cu (130), Fe (10), Mn (3), Mo (20), Si (200), C (70), N (210), O (340)
53-3Z	Ni_{53}-Ti_{44}-Zr_3	57.1 [53.6]	37.6 [43.3]	5.17 Zr [3.12]	Cu (40), Fe (10), Mn (5), Mo (20), Si (190), C (70), N (2), O (240)
54-3Z	Ni_{54}-Ti_{43}-Zr_3	57.8 [54.4]	36.7 [42.4]	5.25 Zr [3.18]	Cu (80), Fe (10), Mn (8), Mo (20), Si (800), C (60), N (10), O (260)
55-3Z	Ni_{55}-Ti_{42}-Zr_3	58.9 [55.5]	35.7 [41.3]	5.26 Zr [3.19]	Cu (<10), Fe (15), Mn (2), Mo (20), Si (670), C (60), N (2), O (200)
52-5H	Ni_{52}-Ti_{43}-Hf_5	50.8 [52.1]	34.0 [42.8]	14.9 Hf [5.02]	Al (30), Cu (20), Fe (10), Mo (20), Zr (2000), C (60), N (<10), O (150)
53-5H	Ni_{53}-Ti_{42}-Hf_5	51.0 [52.4]	33.8 [42.5]	14.9 Hf [5.03]	Al (20), Cu (40), Fe (30), Mo (20), Zr (2100), C (75), N (25), O (235)
54-5H	Ni_{54}-Ti_{41}-Hf_5	52.6 [54.1]	32.3 [40.8]	14.8 Hf [5.00]	Al (20), Cu (20), Fe (20), Mo (20), Zr (2100), C (60), N (<10), O (140)
55-5H	Ni_{55}-Ti_{40}-Hf_5	53.5 [55.0]	31.6 [39.9]	14.6 Hf [4.95]	Al (10), Co (20), Cu (90), Fe (10), Mo (20), W (100), Zr (2100), C (74), N (24), O (240)

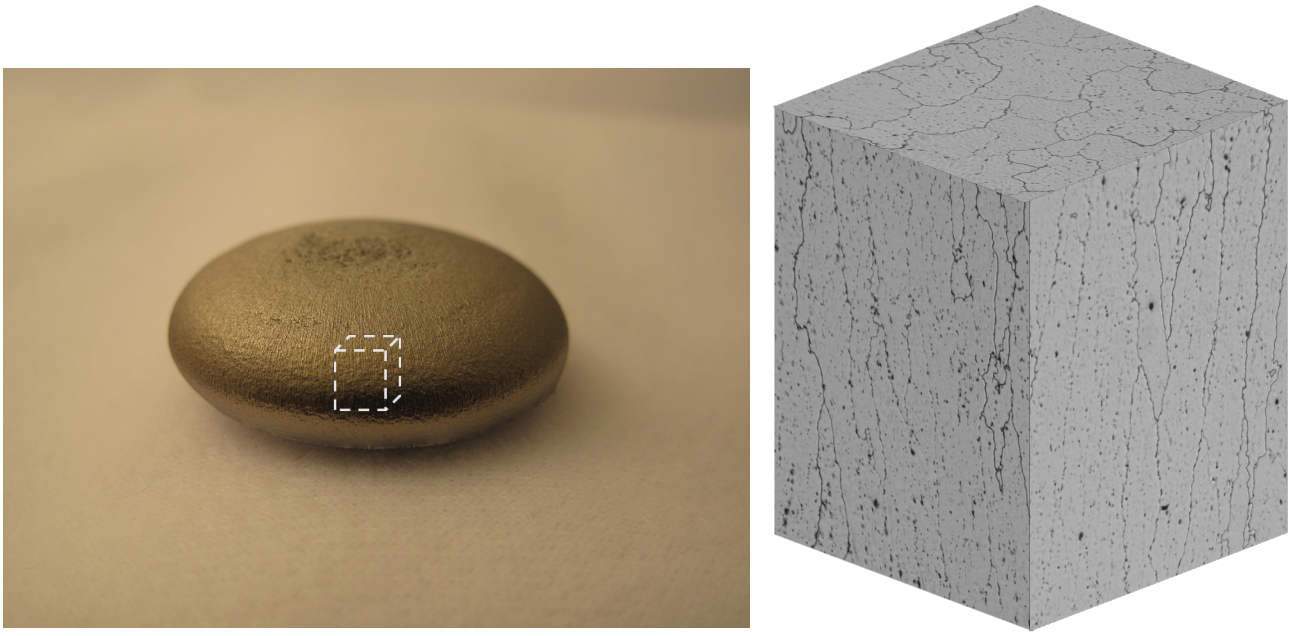

(a) (b)

Figure 1.—(a) Example of a Ni-Ti button fabricated by vacuum arc melting and (b) representative microstructure of the material in the orientations indicated by the cube in (a). The orientation of the grains, which tends to be orthogonal to the bottom of the crucible, obeys the customary solidification kinetics, aligning in the direction of heat removal.

Commercially available image analysis software was used to calculate the percentage of second phase present in each compound. A total area of approximately 9×10^5 μm^2 was analyzed for each specimen. The image analysis was performed at a magnification of 200× and the software measurement system was calibrated such that each pixel corresponded to approximately 0.5 μm both vertically and horizontally. Each monochromatic photomicrograph had a bit-depth of 8 bits per pixel with an image resolution of 1,360 by 1,024 pixels. Thresholding was selected between 170 (grey) and 255 (black) so that the secondary phases were distinct from the parent phase. A typical example of a microstructure and the accompanying analyzed image is shown in Figure 2. Due to the very consistent grey level of the parent phase, it was possible to compute its coverage area, excluding the lighter shades of grey comprising the secondary phases. Please note that, in this document, all phases other than parent phase NiTi are classified with the general term "secondary phases." In the binary alloy, these phases primarily consisted of Ni_3Ti, Ni_4Ti_3, possibly small amounts of Ni_3Ti_2, and very small quantities of oxides and carbides, based upon previous studies (Refs. 11 and 12). An analysis of the composition of the phases present in the ternary alloys will be presented in future publications.

Vickers microindentation hardness was measured using standard procedures (Ref. 13). Unlike the standard method, however, a linear indentation spacing of 500 μm was used to eliminate any near-field strain-hardening, which was found to be an issue with this material. Care was taken to avoid making indentations on clusters of precipitate phase material as this tended to distort the edges of the indentations. The average of five to seven hardness measurements at every heat treatment condition is reported for each alloy to allow for removal of outlying data points.

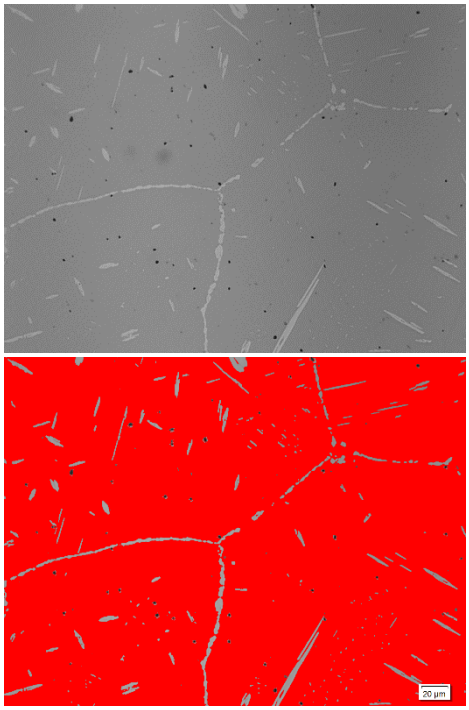

Figure 2.—(a) Optical micrograph and (b) corresponding image after conversion for image analysis showing the parent phase in red and the precipitate phases in grey. The specimen is alloy 55-1H (55 at.% Ni – 44 at.% Ti – 1 at.% Hf) afer heat treatment at 900 °C for 2 hr (water quench) and the secondary phase comprises approximately 4 percent in this image.

Results

Microstructures

Optical micrographs of each of the studied compounds are shown in Figures 3 through 30.

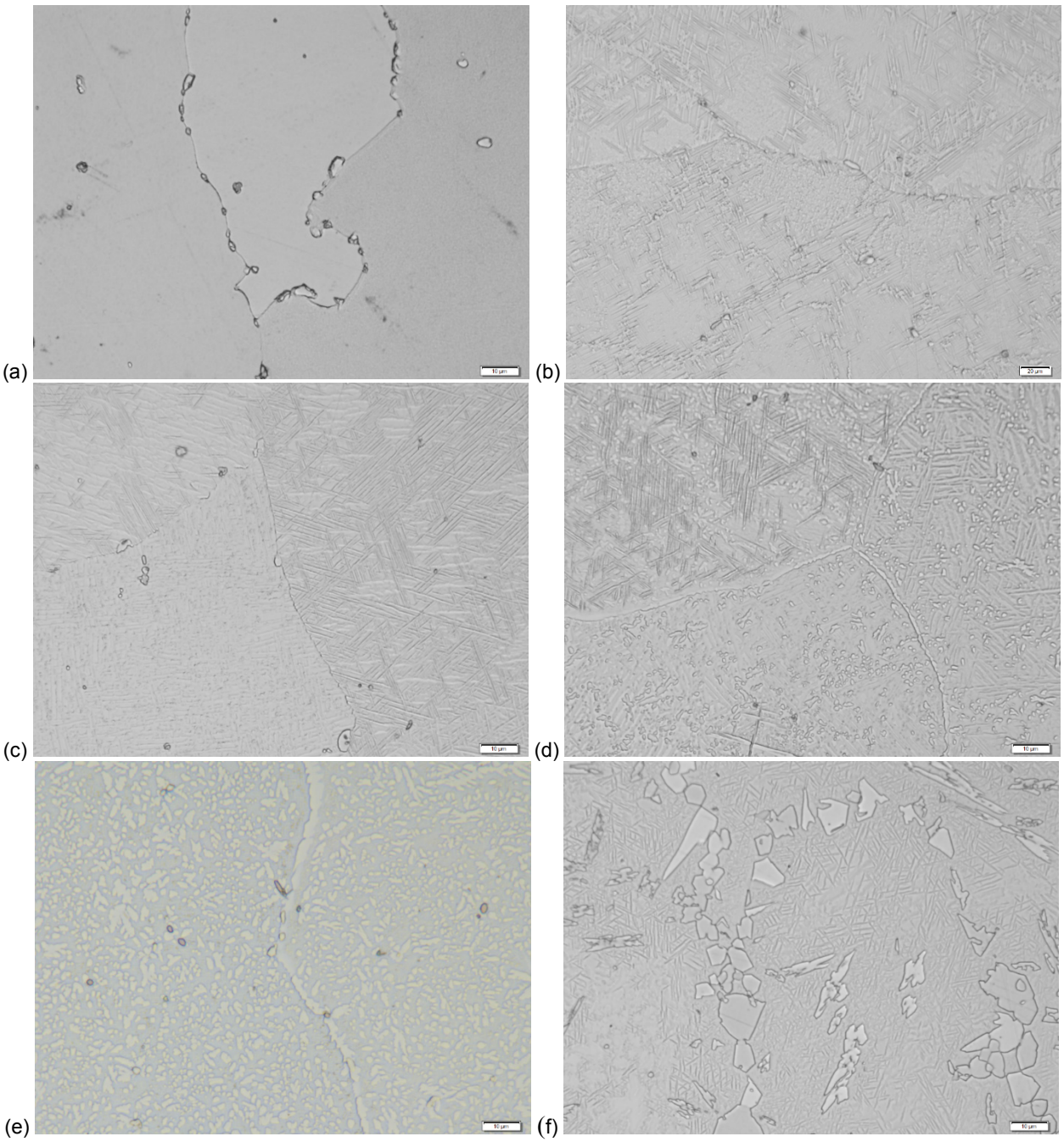

Figure 3.—Brightfield optical photomicrographs showing alloys (a) 51, (b) 52, (c) 53, (d) 54, (e) 55, and (f) 56 after homogenization at 1,050 °C for 48 hr followed by furnace cooling. The homogenized microstructure represents an equilibrium microstructure. Work is underway to identify the fine phases.

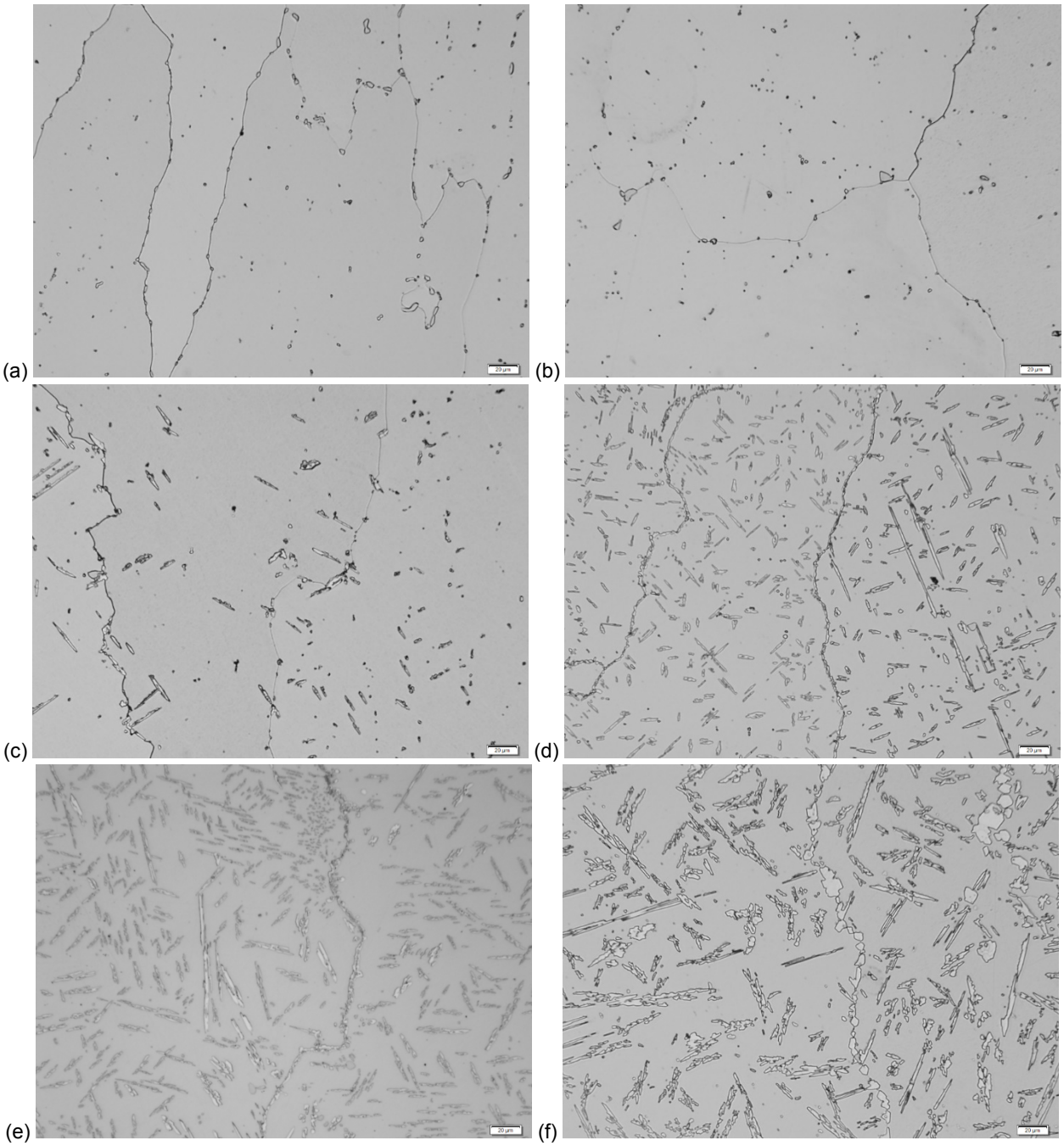

Figure 4.—Brightfield optical photomicrographs showing alloys (a) 51, (b) 52, (c) 53, (d) 54, (e) 55, and (f) 56 after heat treatment at 800 °C for 2 hr (water quench). The photomicrographs show the increase of second phase with increasing Ni content from (a) to (f).

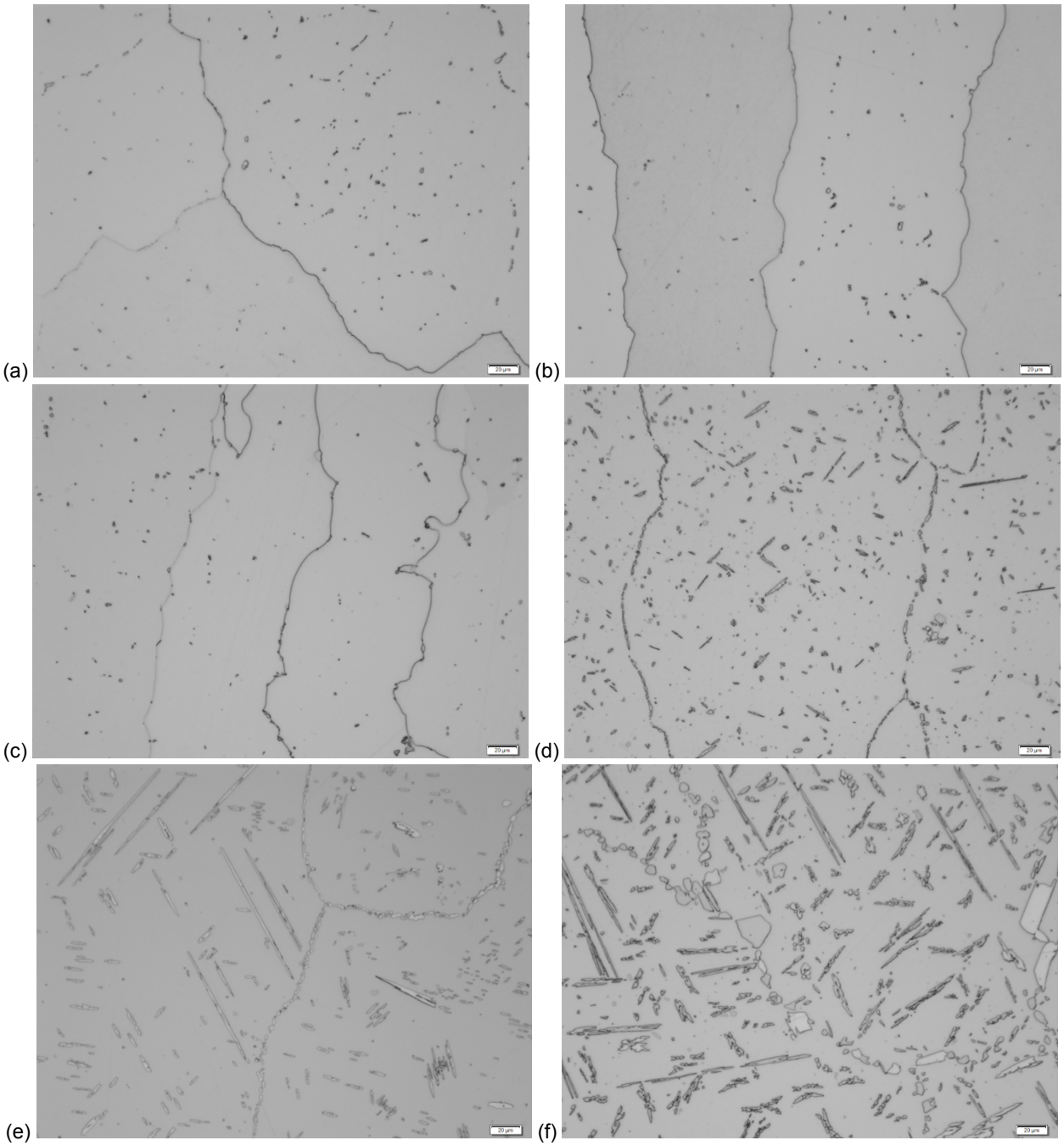

Figure 5.—Brightfield optical photomicrographs showing alloys (a) 51, (b) 52, (c) 53, (d) 54, (e) 55, and (f) 56 after heat treatment at 900 °C for 2 hr (water quench). The photomicrographs show the increase of second phase with increasing Ni content from (a) to (f).

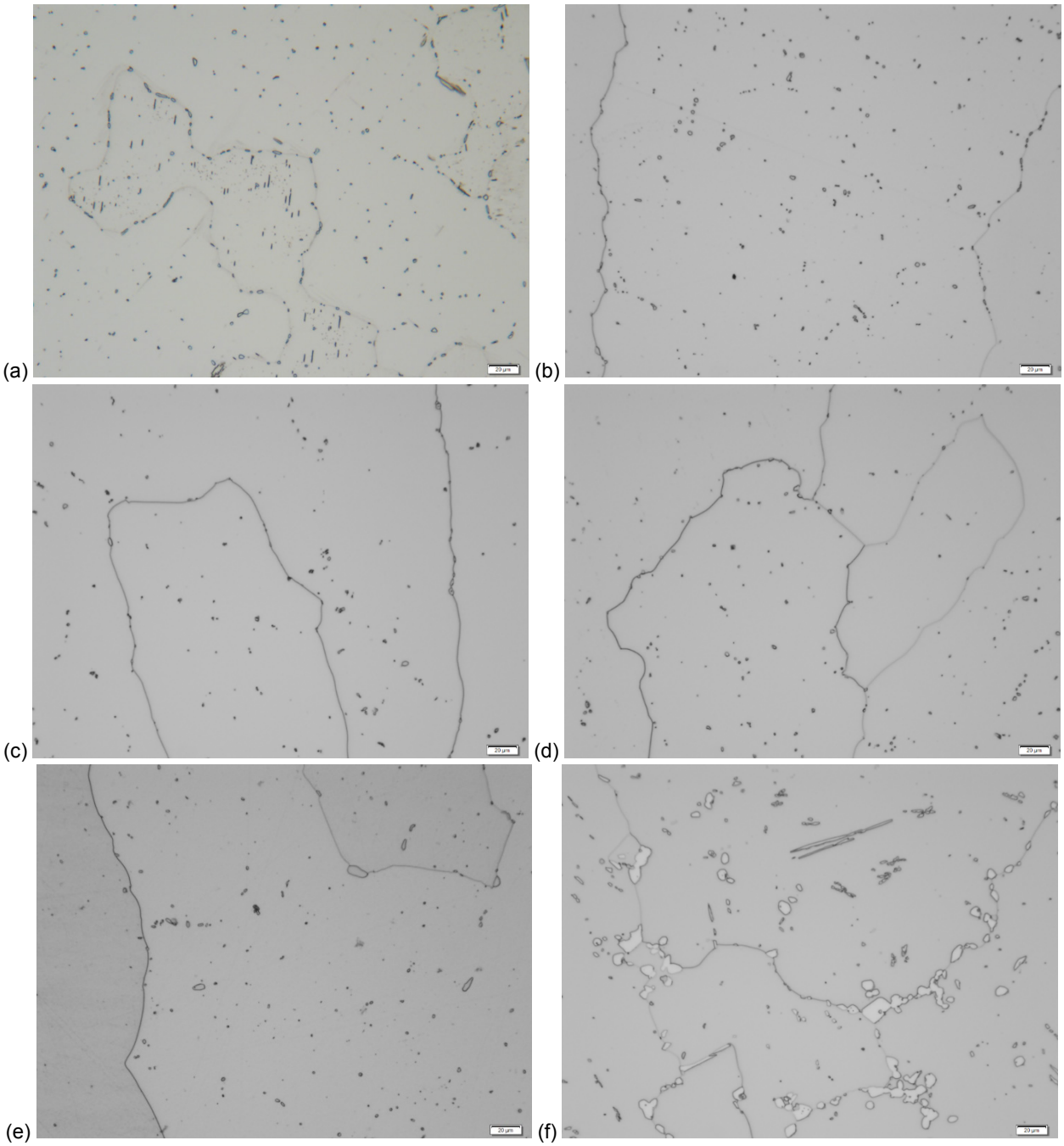

Figure 6.—Brightfield optical photomicrographs showing alloys (a) 51, (b) 52, (c) 53, (d) 54, (e) 55, and (f) 56 after heat treatment at 1,000 °C for 2 hr (water quench). At this temperature, the only compound to generate precipitates was alloy 56 (e). After this heat treatment, only negligible amounts of secondary phases remain except with alloy 56 (e).

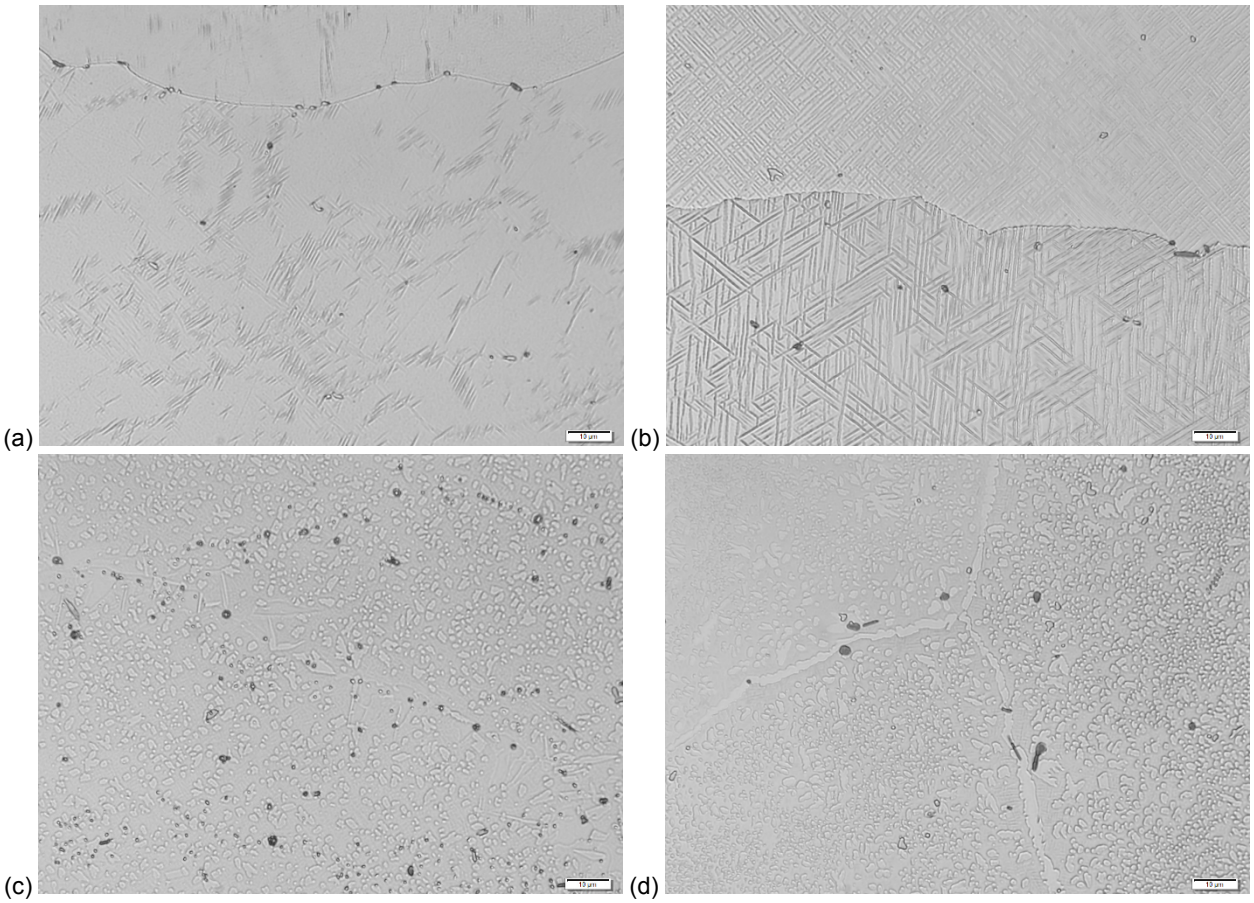

Figure 7.—Optical micrographs of alloys (a) 52-1H, (b) 53-1H, (c) 54-1H, and (d) 55-1H after vacuum homogenization at 1,050 °C and furnace cooling.

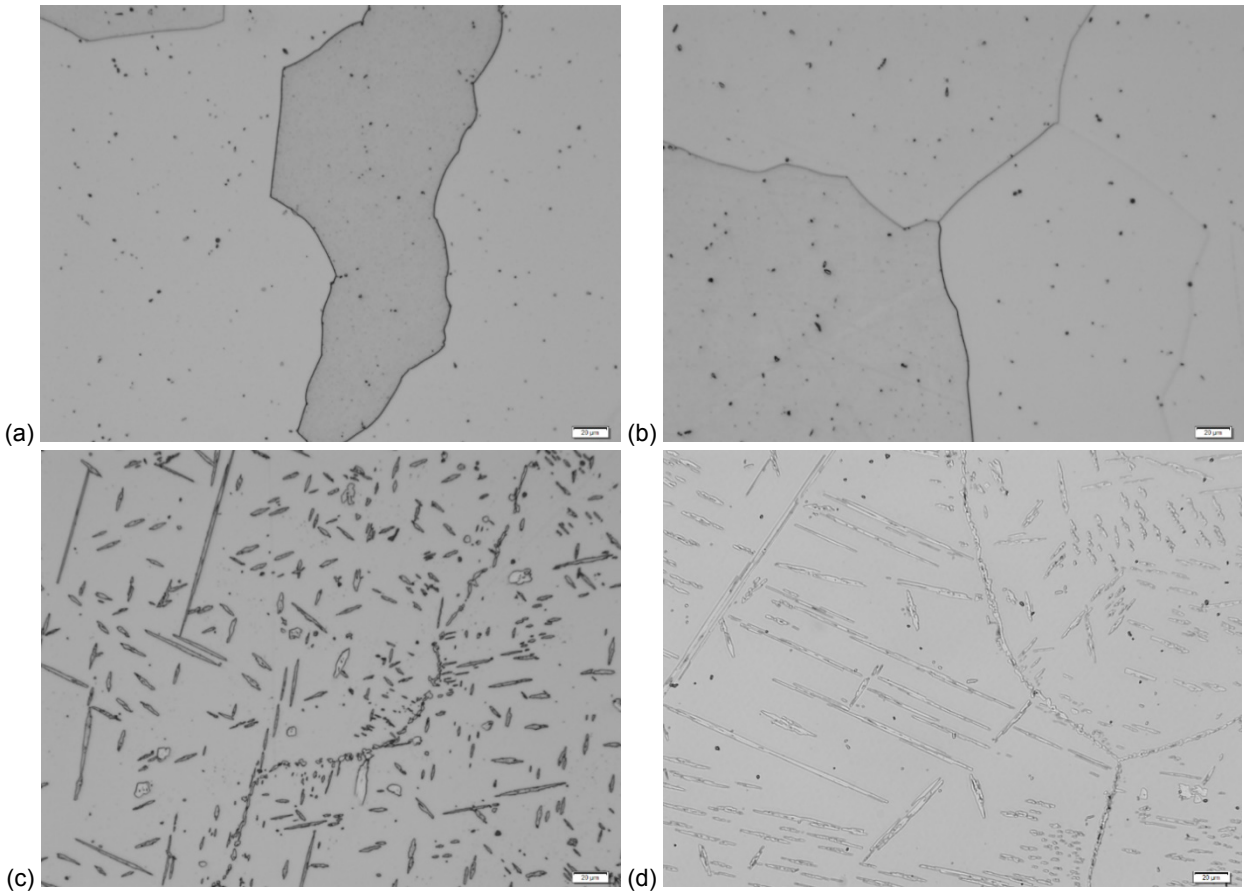

Figure 8.—Optical micrographs of alloys (a) 52-1H, (b) 53-1H, (c) 54-1H, and (d) 55-1H after heat treatment at 800 °C. These photomicrographs show the increase of second phase with increasing Ni content.

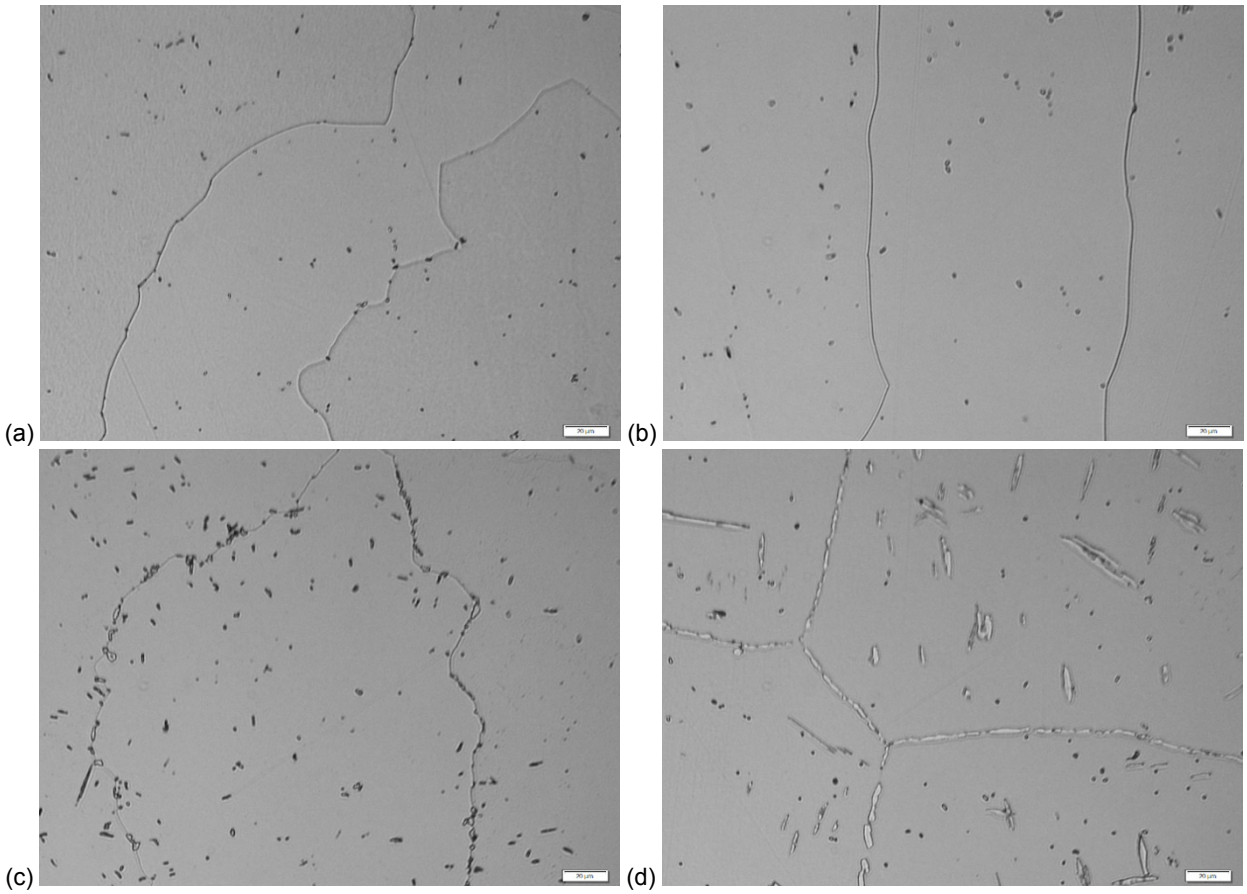

Figure 9.—Optical micrographs of alloys (a) 52-1H, (b) 53-1H, (c) 54-1H, and (d) 55-1H after heat treatment at 900 °C. These photomicrographs show very little increase in second phase with increasing Ni content.

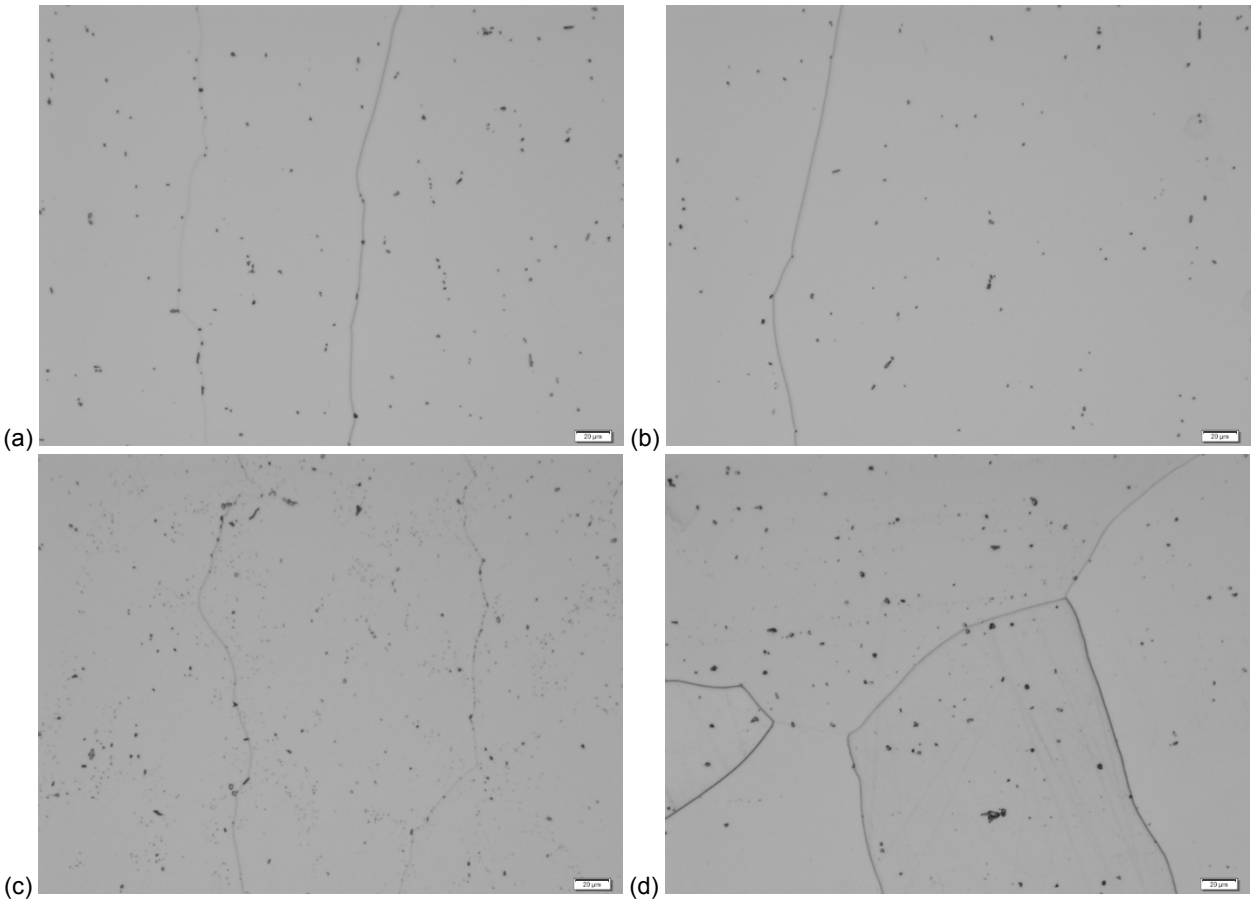

Figure 10.—Optical micrographs of alloys (a) 52-1H, (b) 53-1H, (c) 54-1H, and (d) 55-1H after heat treatment at 1,000 °C. These photomicrographs show that little, if any, precipitation product remains after this heat treatment.

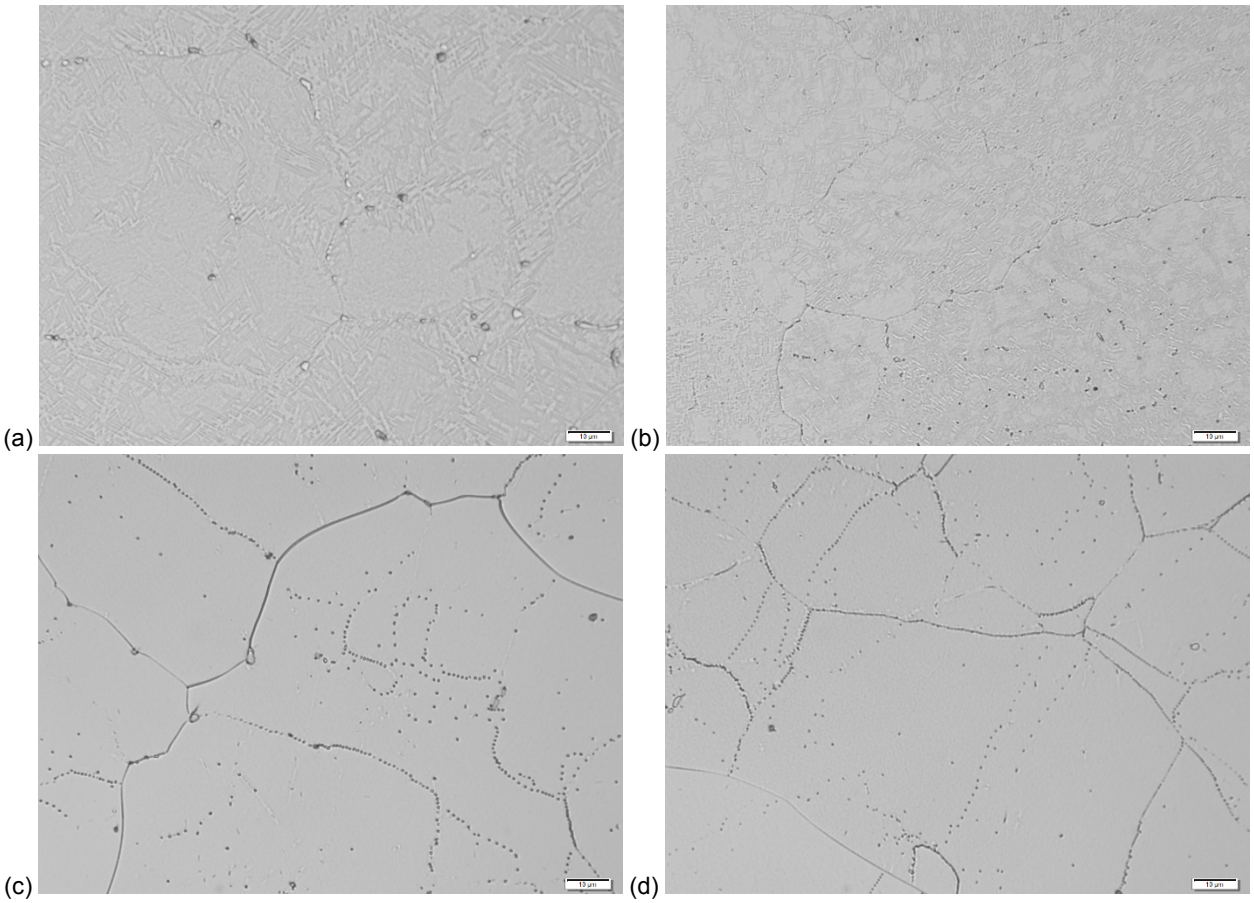

Figure 11.—Photomicrographs showing alloys (a) 52, (b) 52-3T, (c) 52-3H, and (d) 52-3Z after vacuum homogenization at 1,050 °C and furnace cooling.

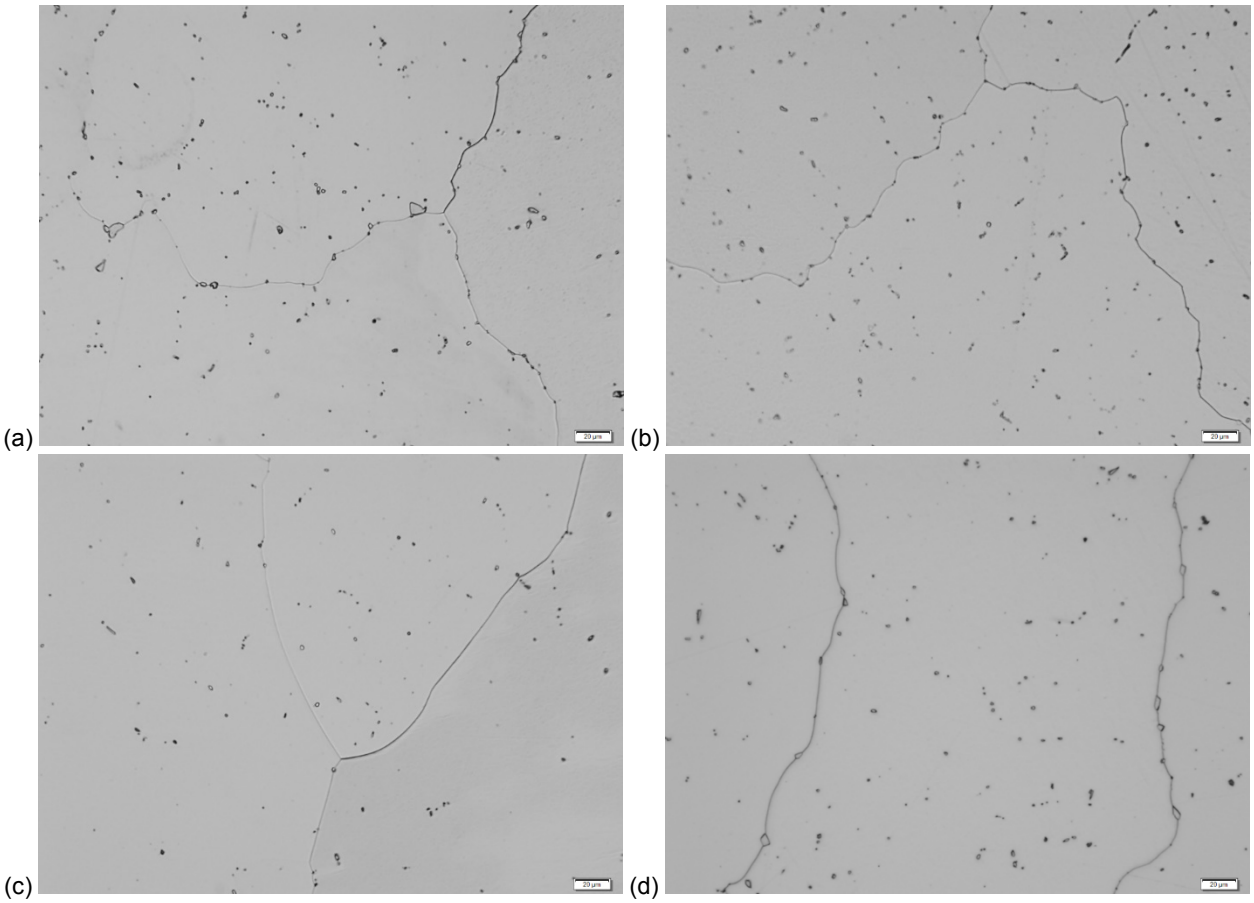

Figure 12.—Photomicrographs showing alloys (a) 52, (b) 52-3T, (c) 52-3H, and (d) 52-3Z after heat treatment at 800 °C. These photomicrographs show that little, if any, precipitation product remains after this heat treatment.

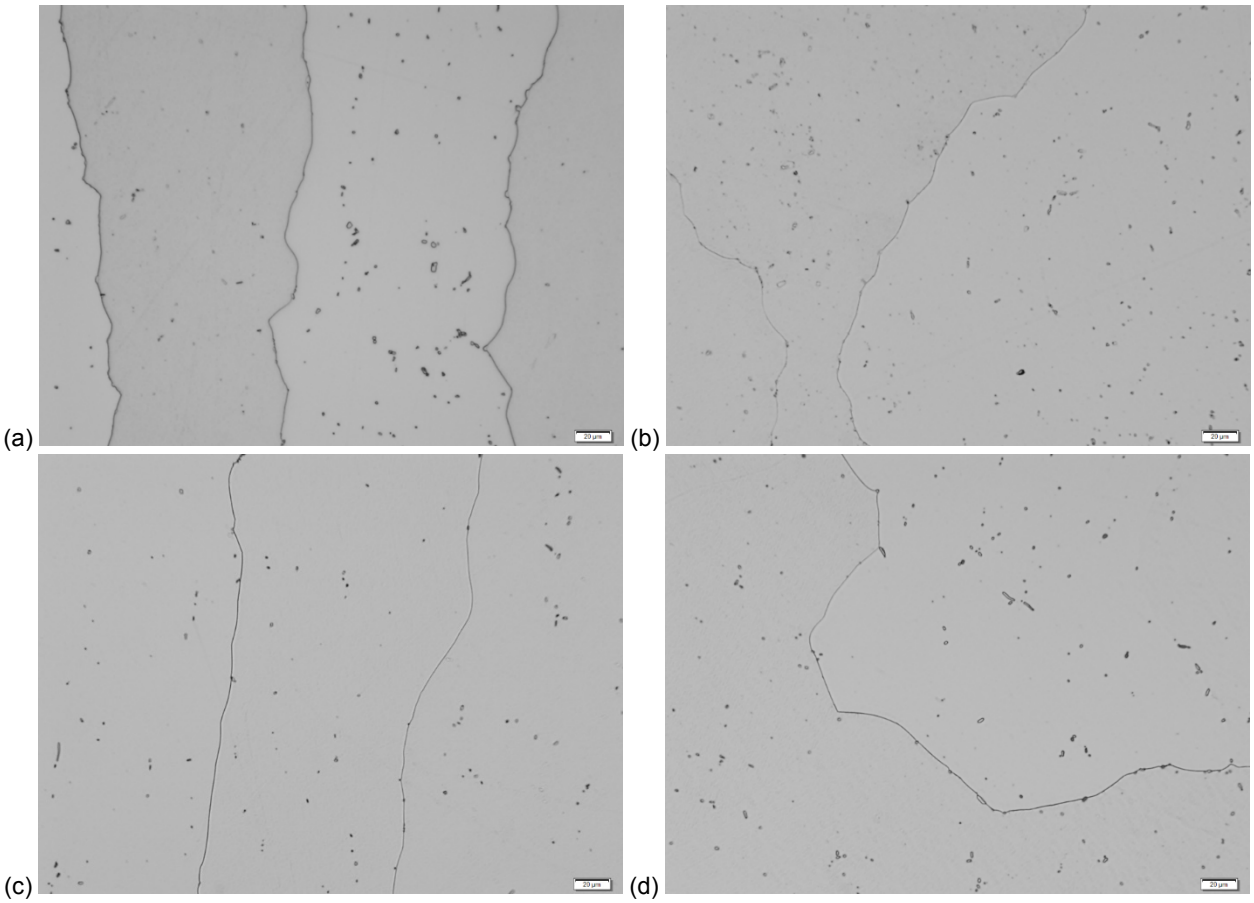

Figure 13.—Photomicrographs showing alloys (a) 52, (b) 52-3T, (c) 52-3H, and (d) 52-3Z after heat treatment at 900 °C. These photomicrographs show that little, if any, precipitation product remains after this heat treatment.

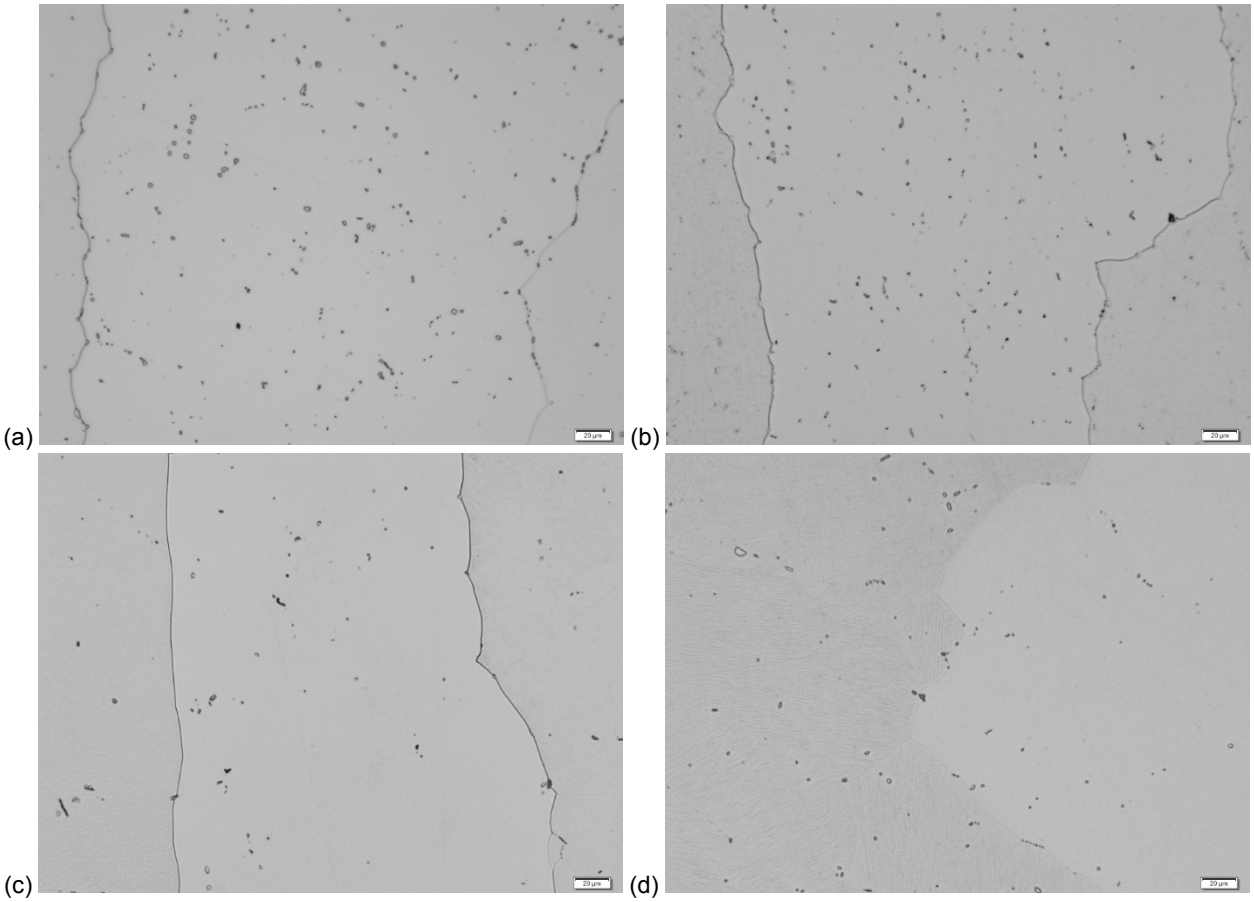

Figure 14.—Photomicrographs showing alloys (a) 52, (b) 52-3T, (c) 52-3H, and (d) 52-3Z after heat treatment at 1,000 °C. These photomicrographs show that little, if any, precipitation product remains after this heat treatment.

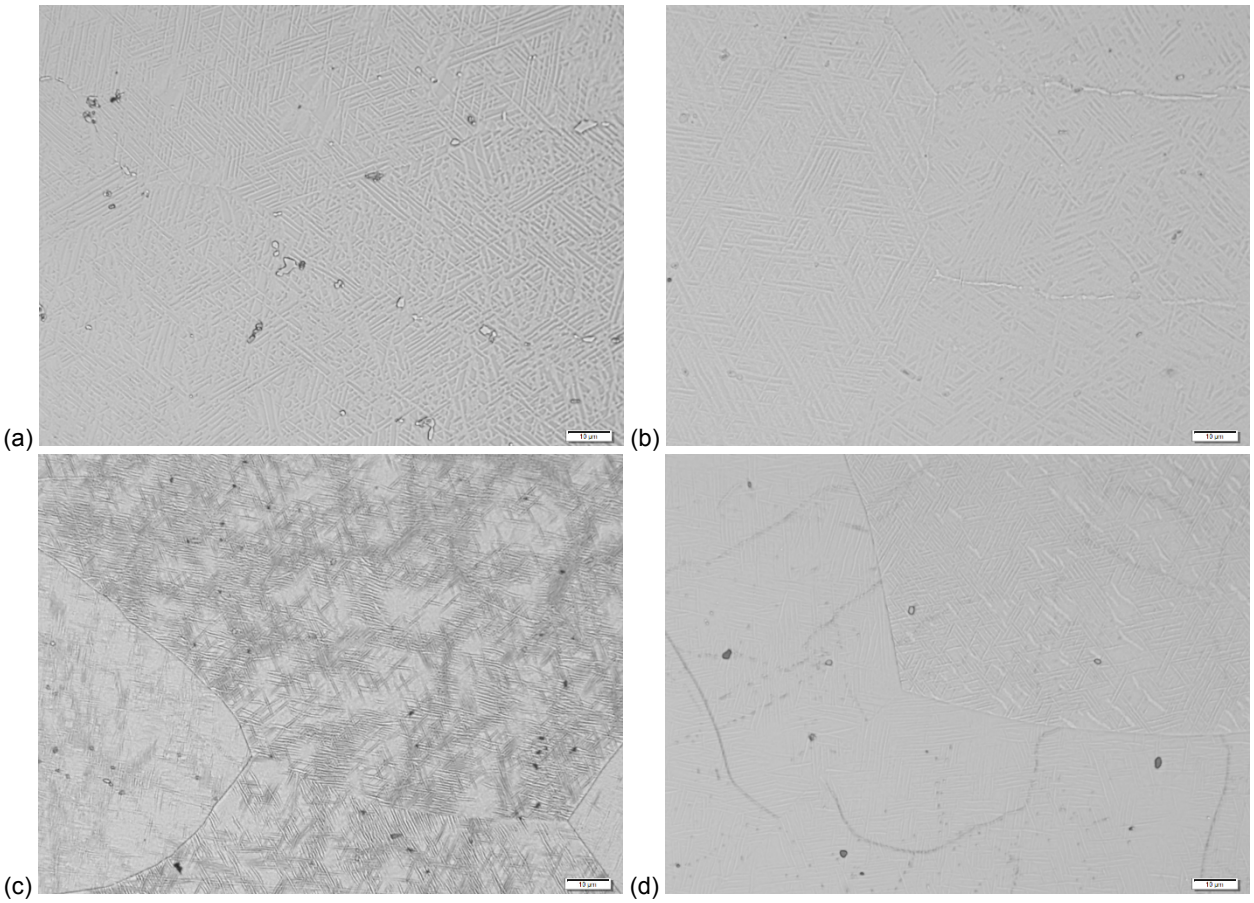

Figure 15.—Photomicrographs showing alloys (a) 53, (b) 53-3T, (c) 53-3H, and (d) 53-3Z after homogenization at 1,050 °C for 48 hr and furnace cooling.

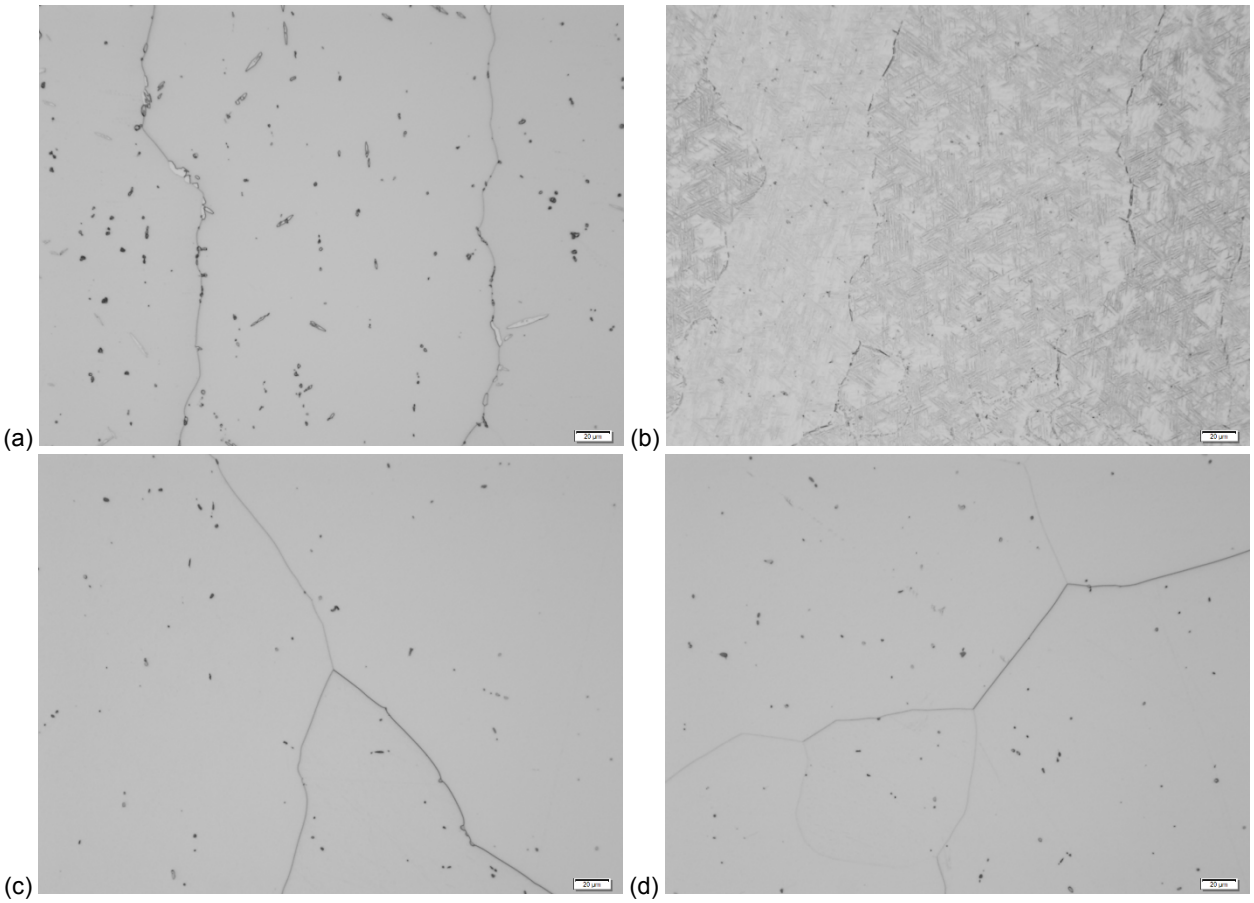

Figure 16.—Photomicrographs showing alloys (a) 53, (b) 53-3T, (c) 53-3H, and (d) 53-3Z after heat treatment at 800 °C. Little, if any, precipitation product is present in alloys 53-3H and 53-3Z (c-d) after this treatment.

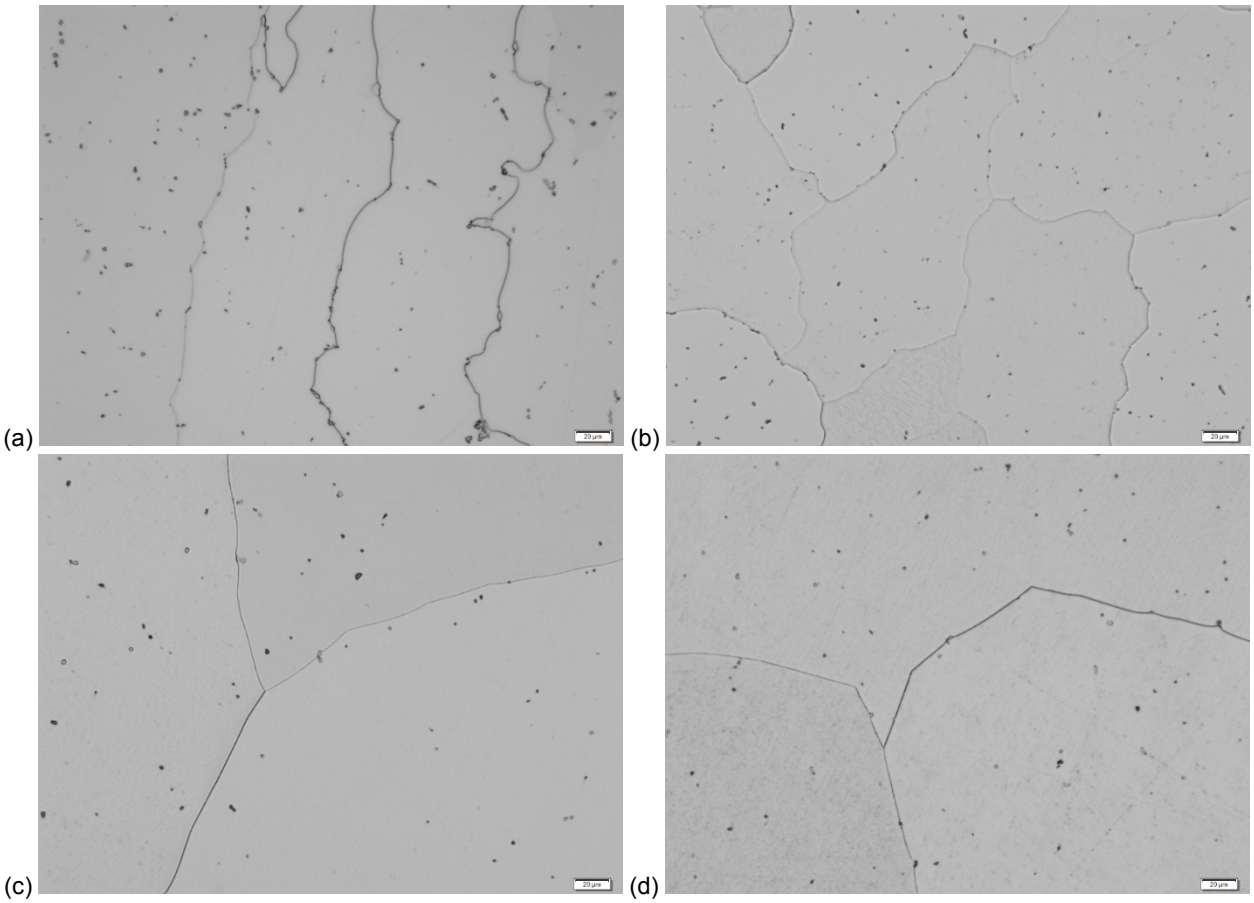

Figure 17.—Photomicrographs showing alloys (a) 53, (b) 53-3T, (c) 53-3H, and (d) 53-3Z after heat treatment at 900 °C. These photomicrographs show that little, if any, precipitation products remain after this heat treatment.

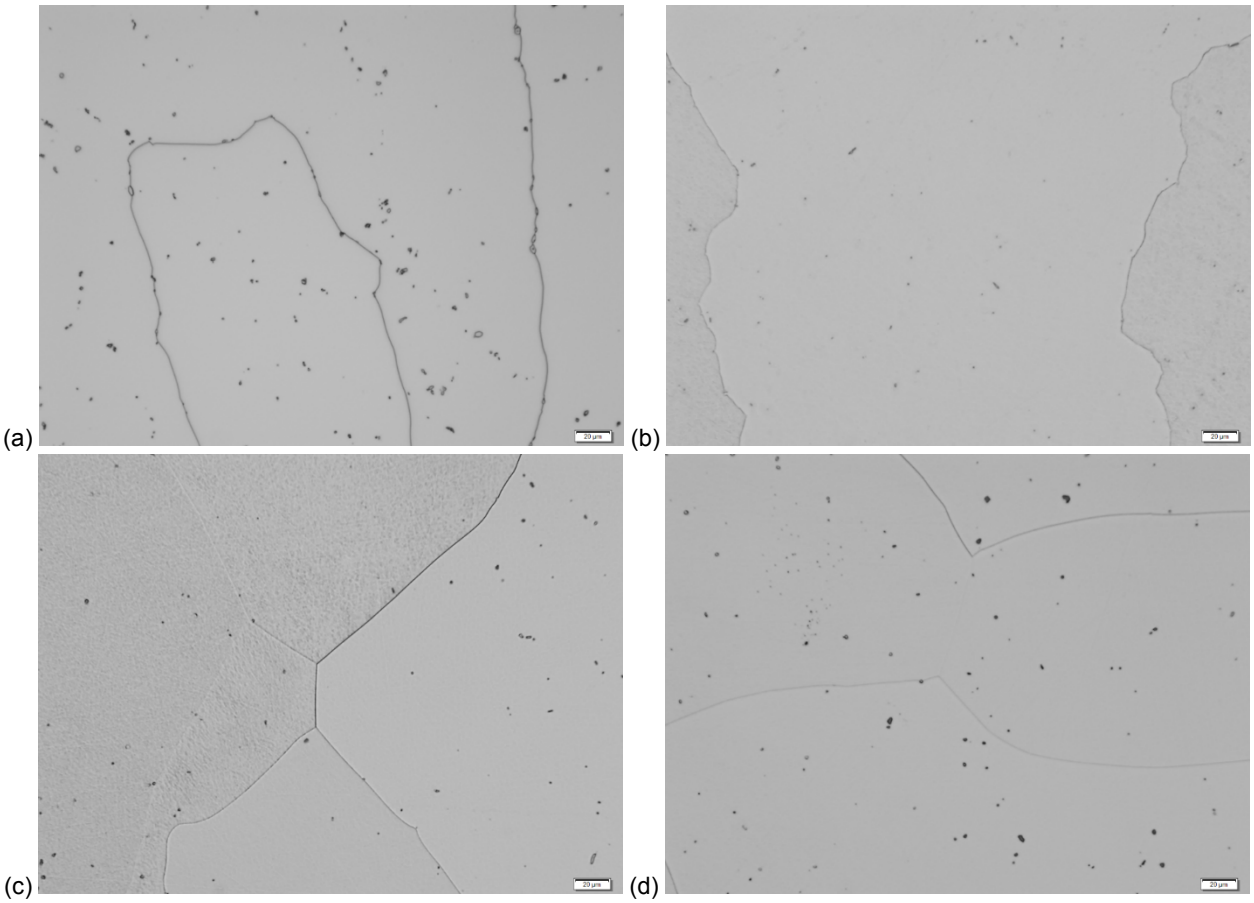

Figure 18.—Photomicrographs showing alloys (a) 53, (b) 53-3T, (c) 53-3H, and (d) 53-3Z after heat treatment at 1,000 °C. These photomicrographs show that little, if any, precipitation products remain after this heat treatment.

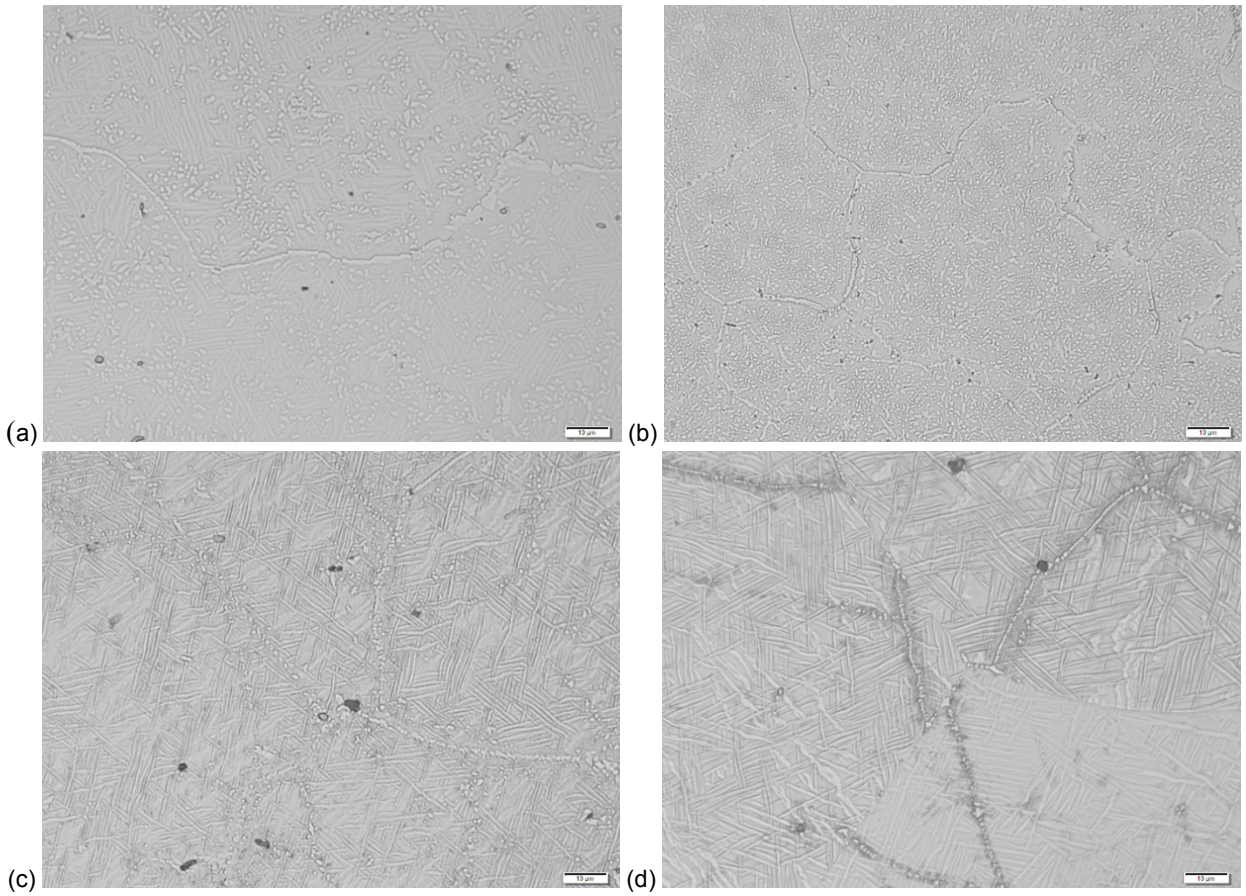

Figure 19.—Photomicrographs showing alloys (a) 54, (b) 54-3T, (c) 54-3H, and (d) 54-3Z after homogenization at 1,050 °C for 48 hr and furnace cooling.

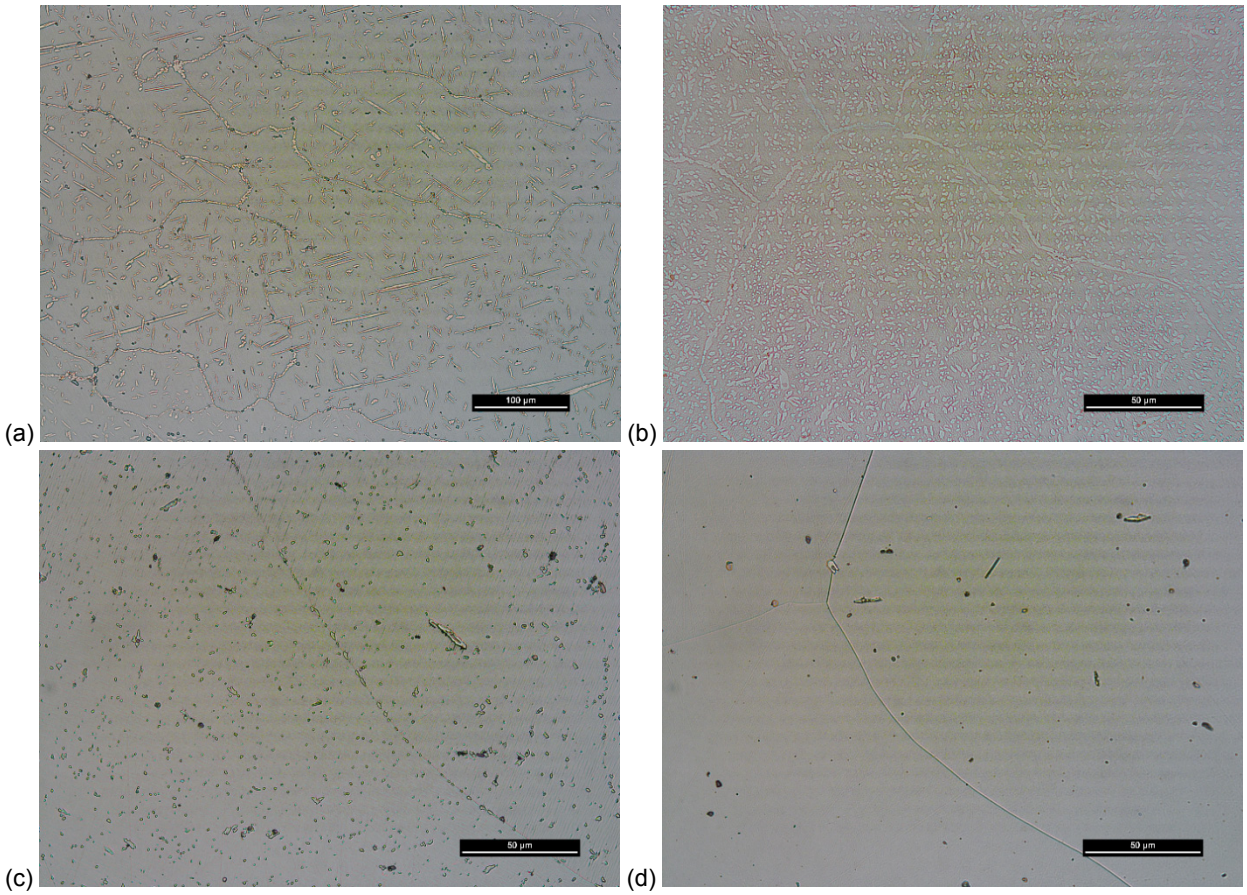

Figure 20.—Photomicrographs showing alloys (a) 54, (b) 54-3T, (c) 54-3H, and (d) 54-3Z after heat treatment at 800 °C. Little, if any, precipitation product remains in alloys 54-3H and 54-3Z (c-d) after this heat treatment.

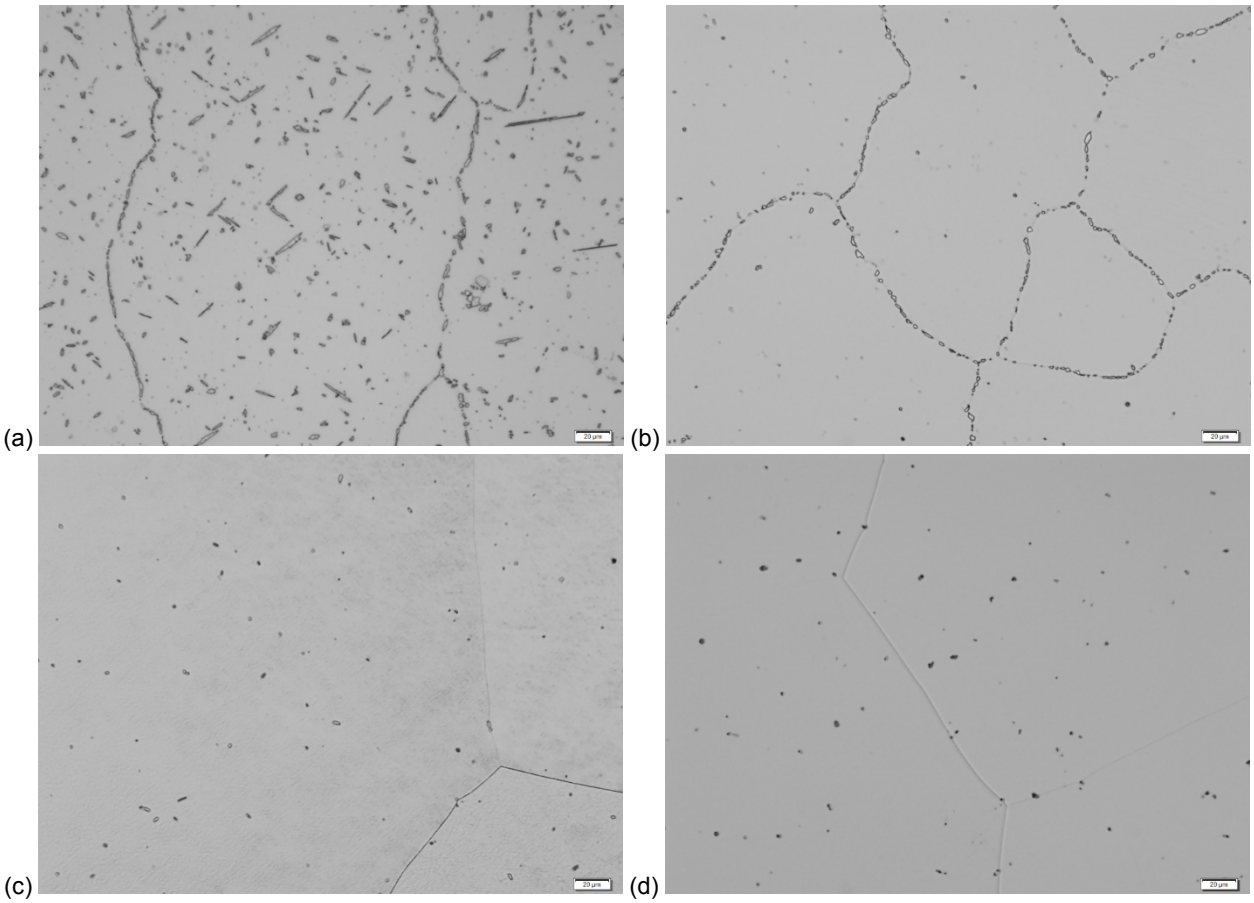

Figure 21.—Photomicrographs showing alloys (a) 54, (b) 54-3T, (c) 54-3H, and (d) 54-3Z after heat treatment at 900 °C. Little, if any, precipitation product remains in alloys 54-3H and 54-3Z (c-d) after heat treatment.

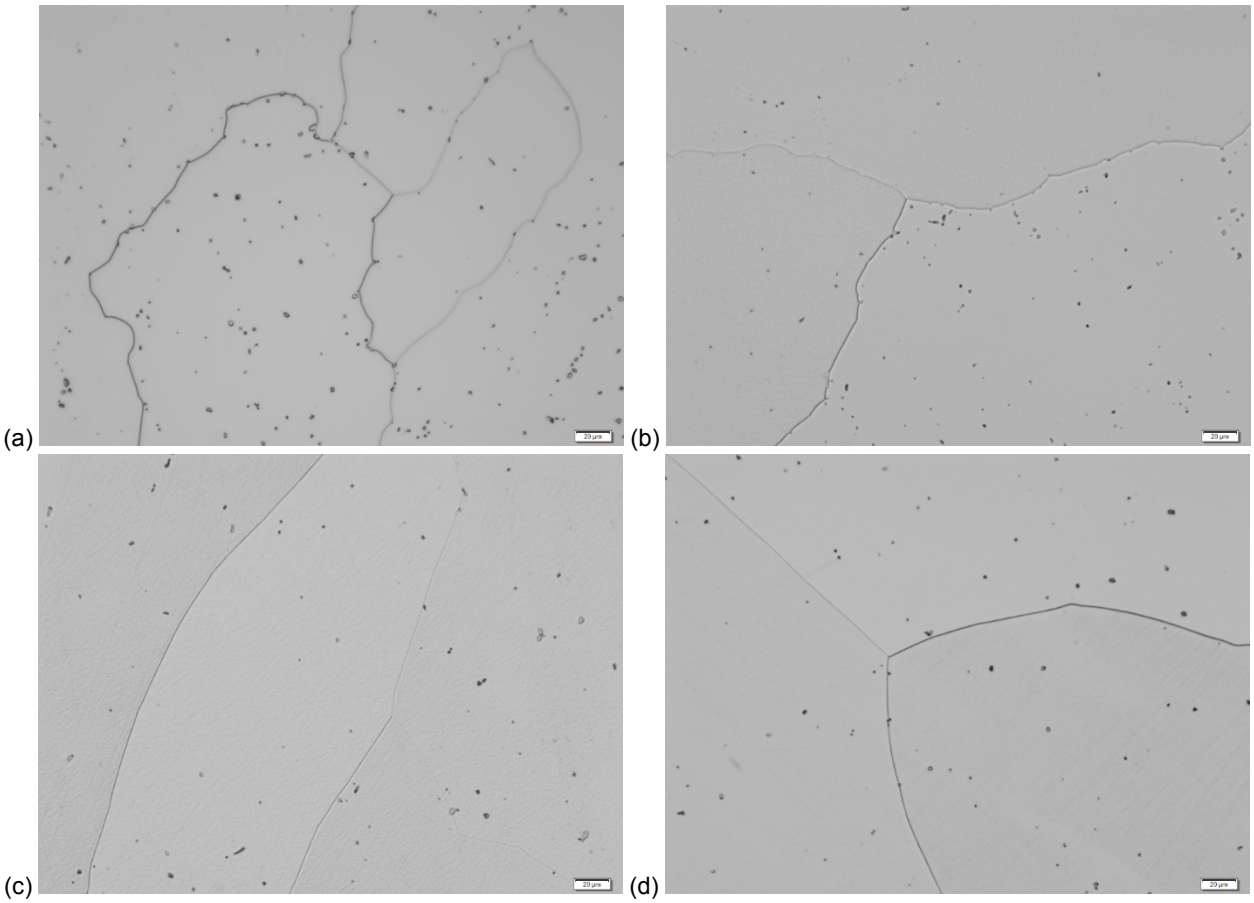

Figure 22.—Photomicrographs showing alloys (a) 54, (b) 54-3T, (c) 54-3H, and (d) 54-3Z after heat treatment at 1,000 °C. These photomicrographs show that essentially no precipitation products remain in these alloys after this heat treatment.

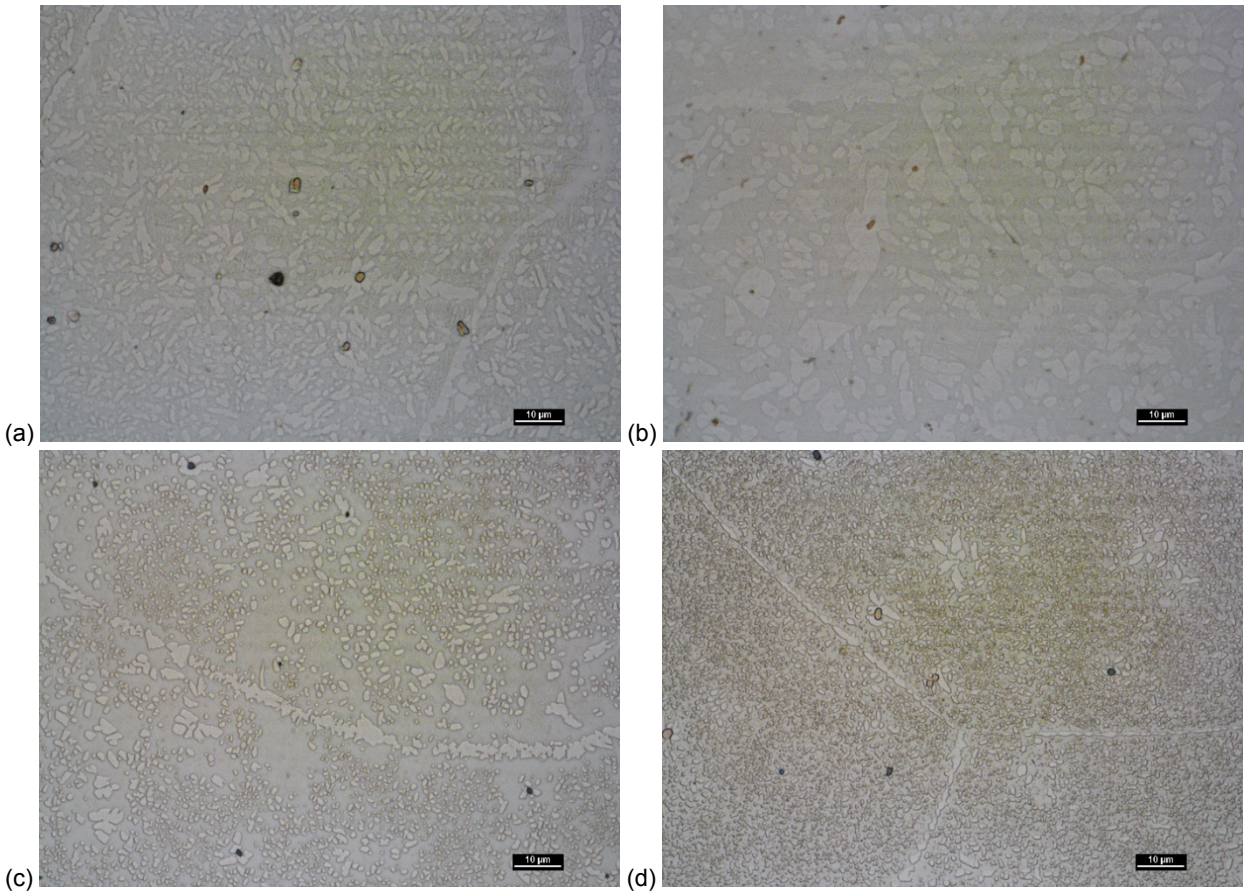

Figure 23.—Brightfield optical photomicrographs showing alloys (a) 55, (b) 55-3T, (c) 55-3H, and (d) 55-3Z after homogenization at 1,050 °C and furnace cooling.

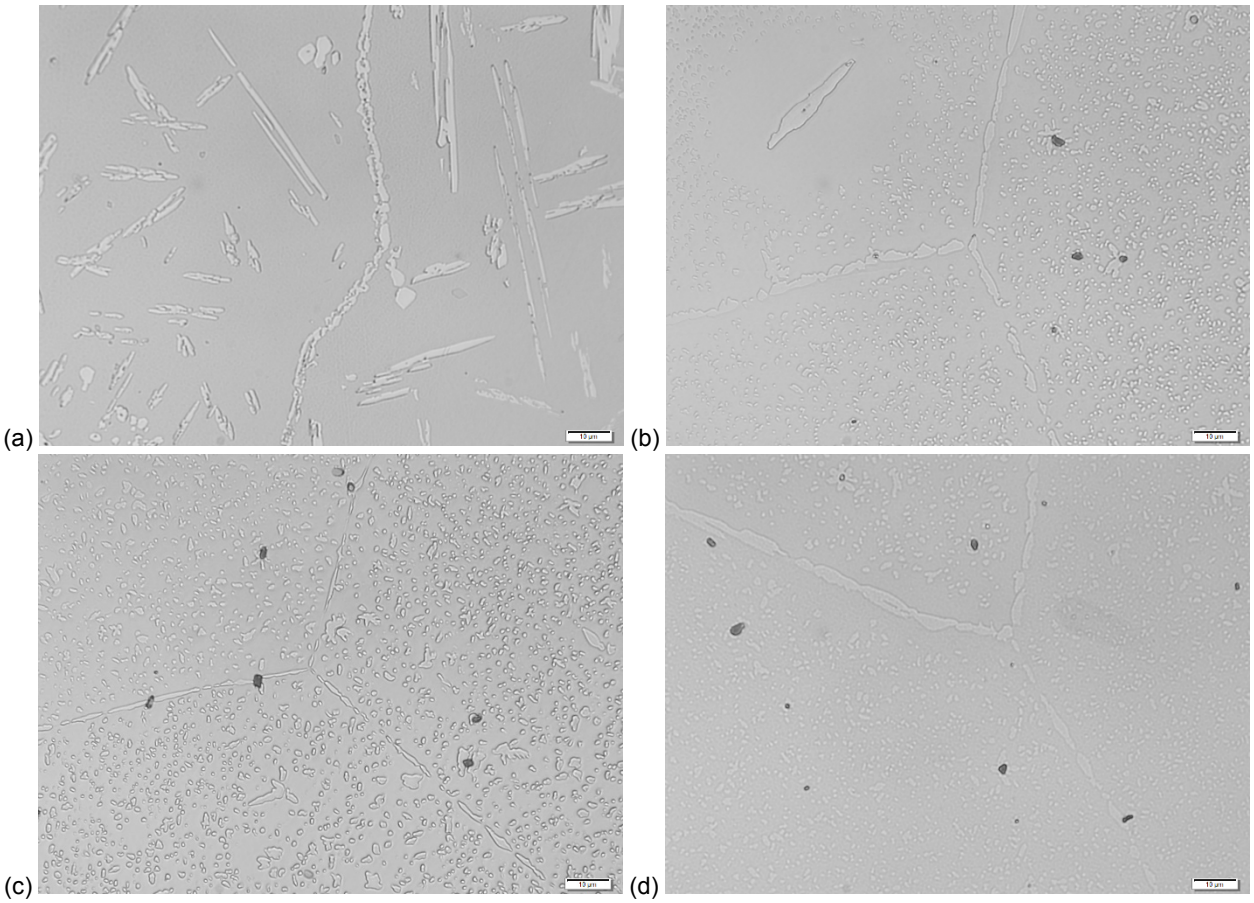

Figure 24.—Photomicrographs showing alloys (a) 55, (b) 55-3T, (c) 55-3H, and (d) 55-3Z after heat treatment at 800 °C.

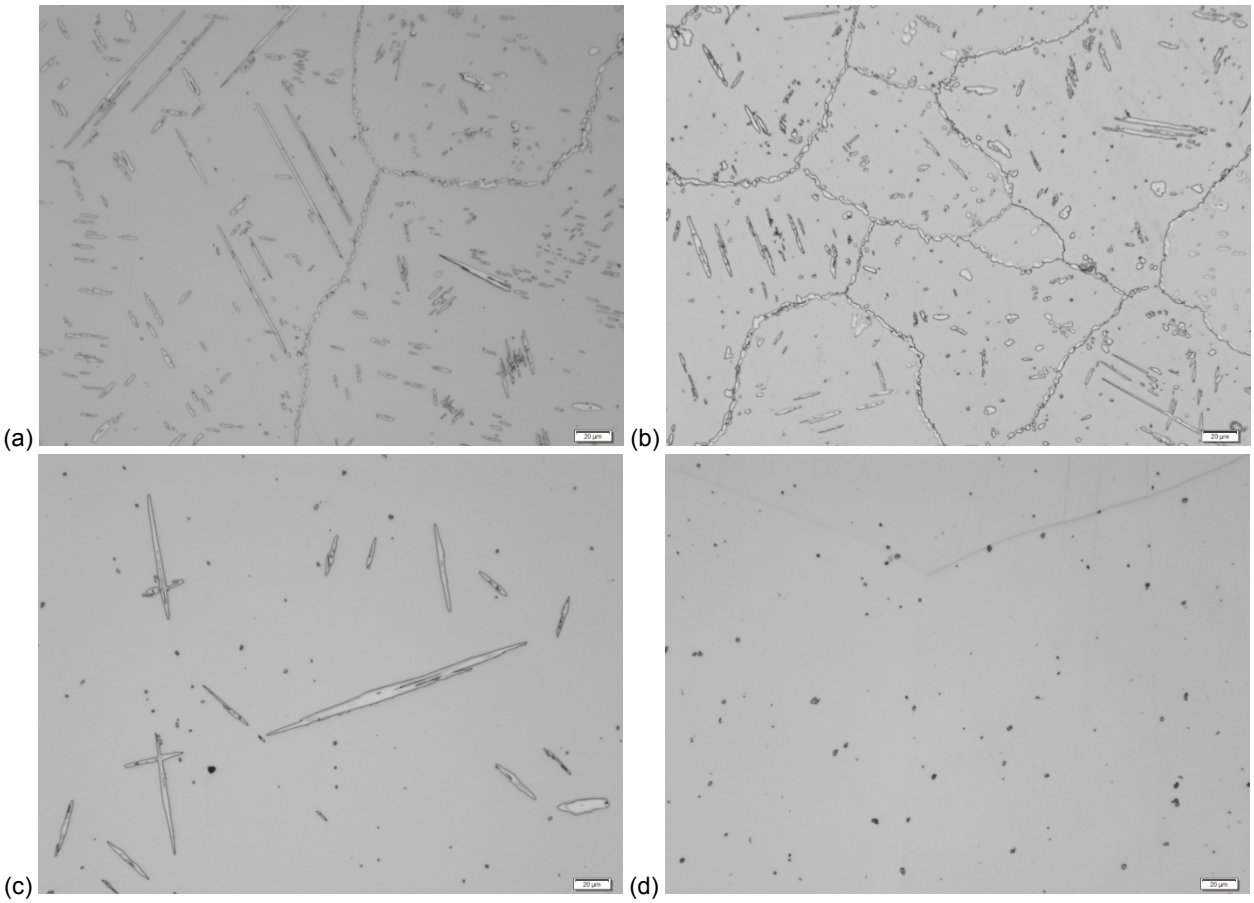

Figure 25.—Photomicrographs showing alloys (a) 55, (b) 55-3T, (c) 55-3H, and (d) 55-3Z after heat treatment at 900 °C. Alloy 55-3Z (d) shows essentially no precipitate formation from this heat treatment (the dark particles are oxides).

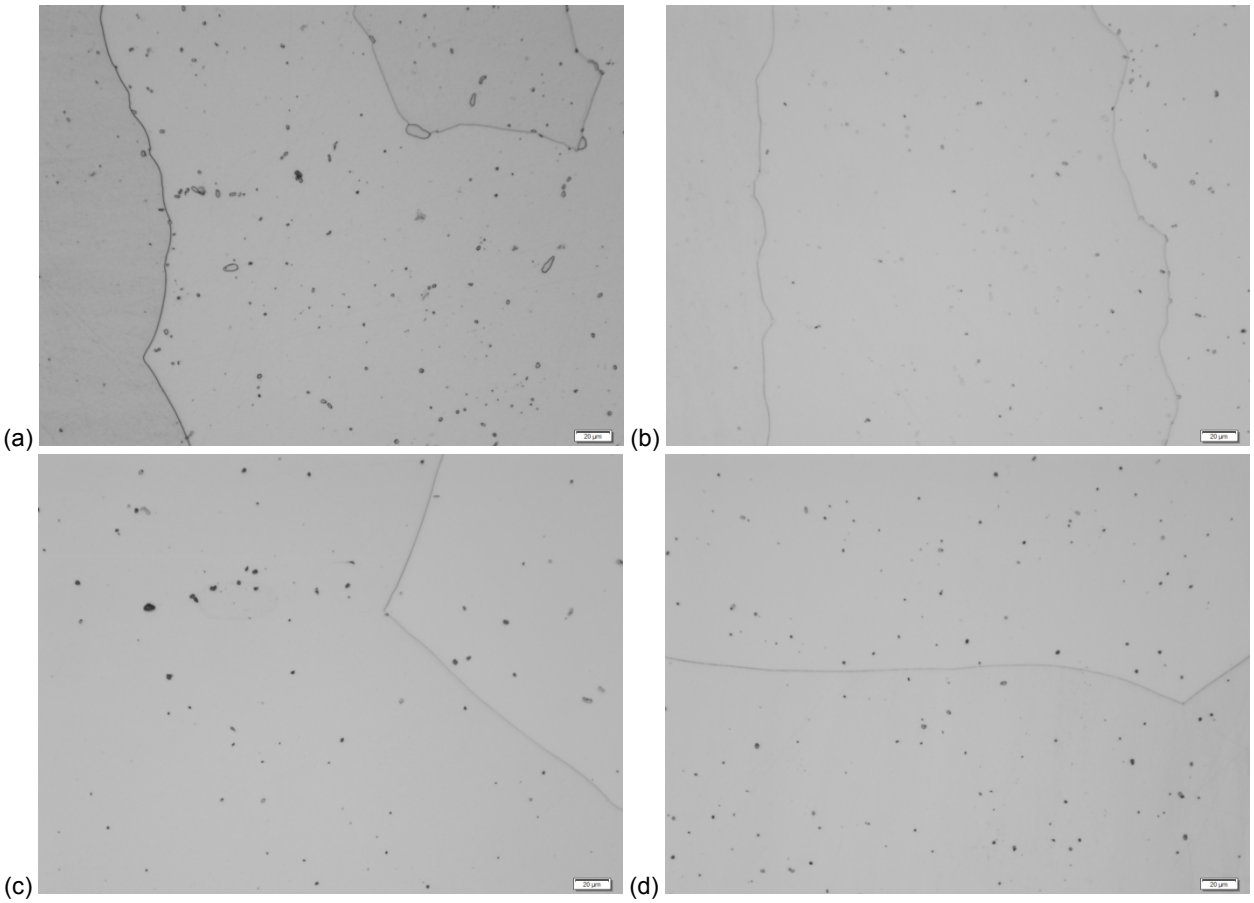

Figure 26.—Photomicrographs showing alloys (a) 55, (b) 55-3T, (c) 55-3H, and (d) 55-3Z after heat treatment at 1,000 °C. These photomicrographs show that essentially no precipitation products are formed in these alloys during this heat treatment.

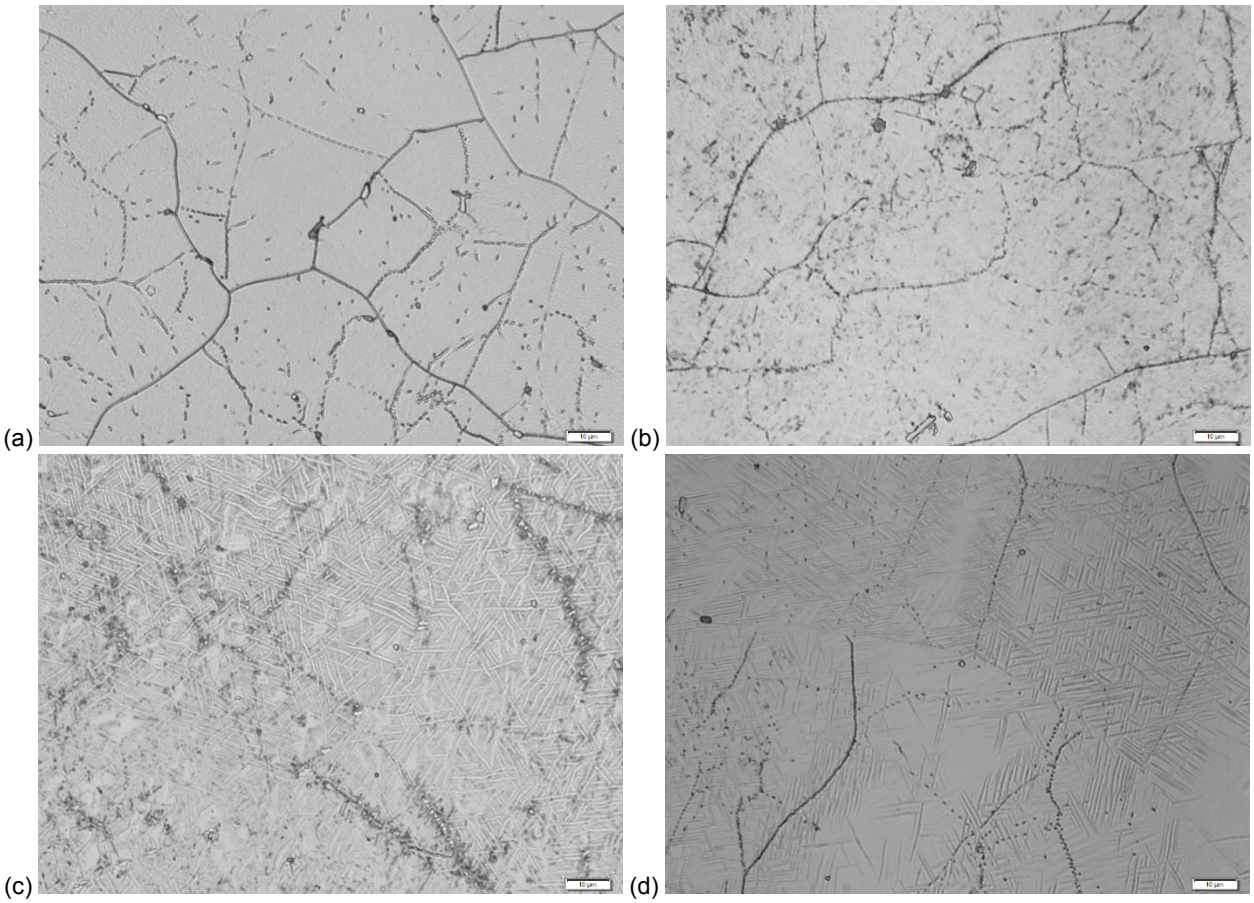

Figure 27.—Photomicrographs showing alloys (a) 52-5H, (b) 53-5H, (c) 54-5H, and (d) 55-5H after homogenization at 1,050 °C for 48 hr and furnace cooling.

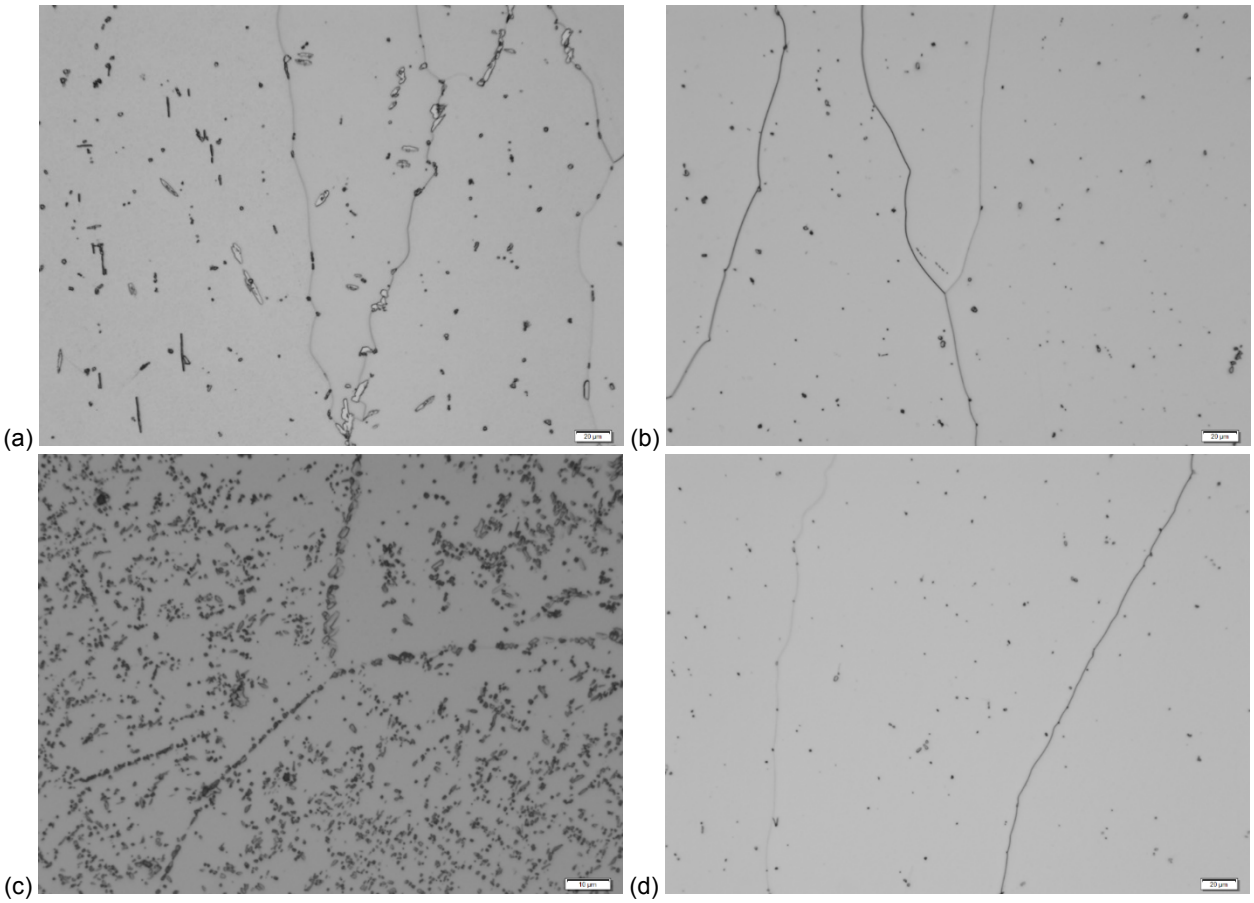

Figure 28.—Photomicrographs showing alloys (a) 52-5H, (b) 53-5H, (c) 54-5H, and (d) 55-5H after heat treatment at 800 °C. Except for alloy 54-5H (c), the microstructures containing 5 at.% Hf had little, if any, precipitation product during this heat treatment.

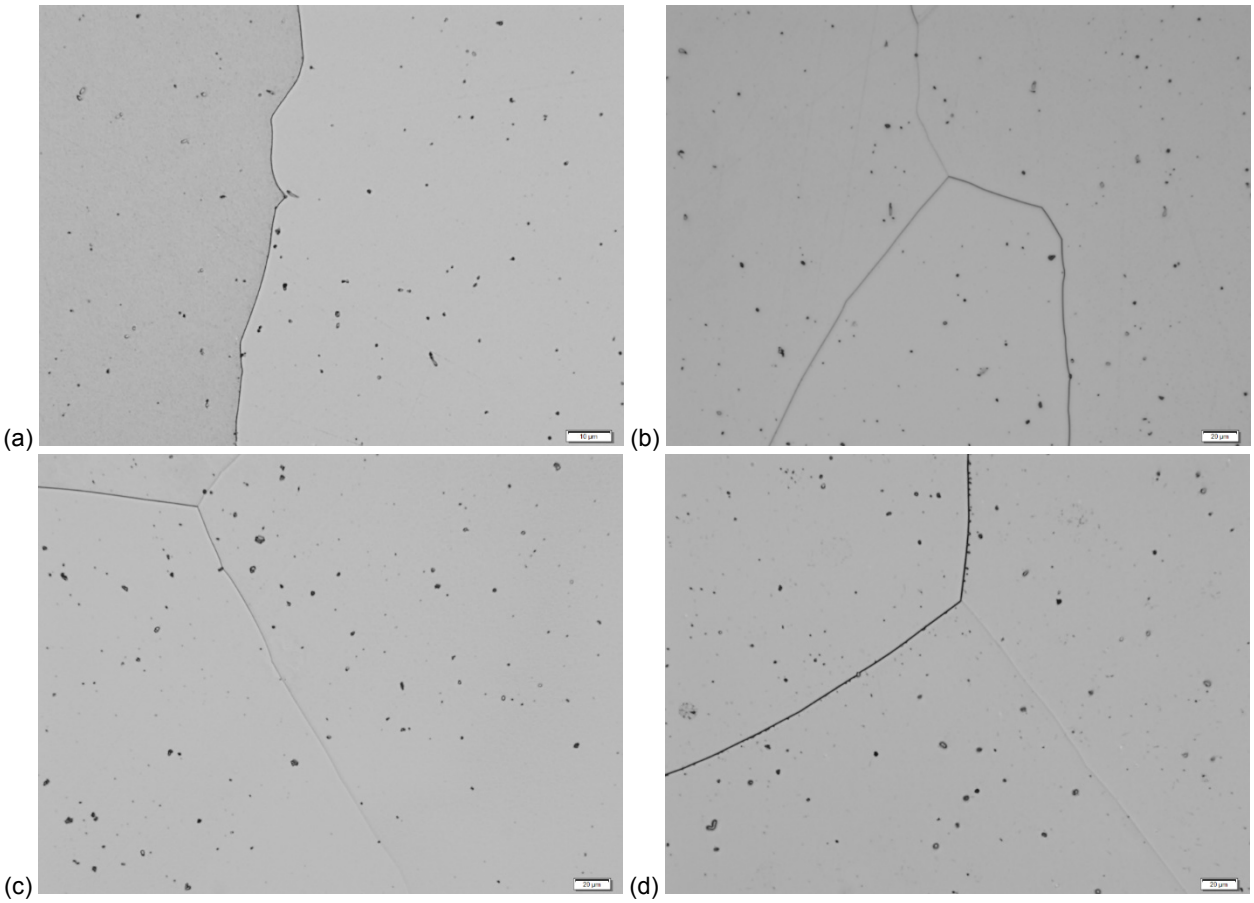

Figure 29.—Photomicrographs showing alloys (a) 52-5H, (b) 53-5H, (c) 54-5H, and (d) 55-5H after heat treatment at 900 °C. These photomicrographs show that essentially no precipitation products are formed in these alloys during this heat treatment.

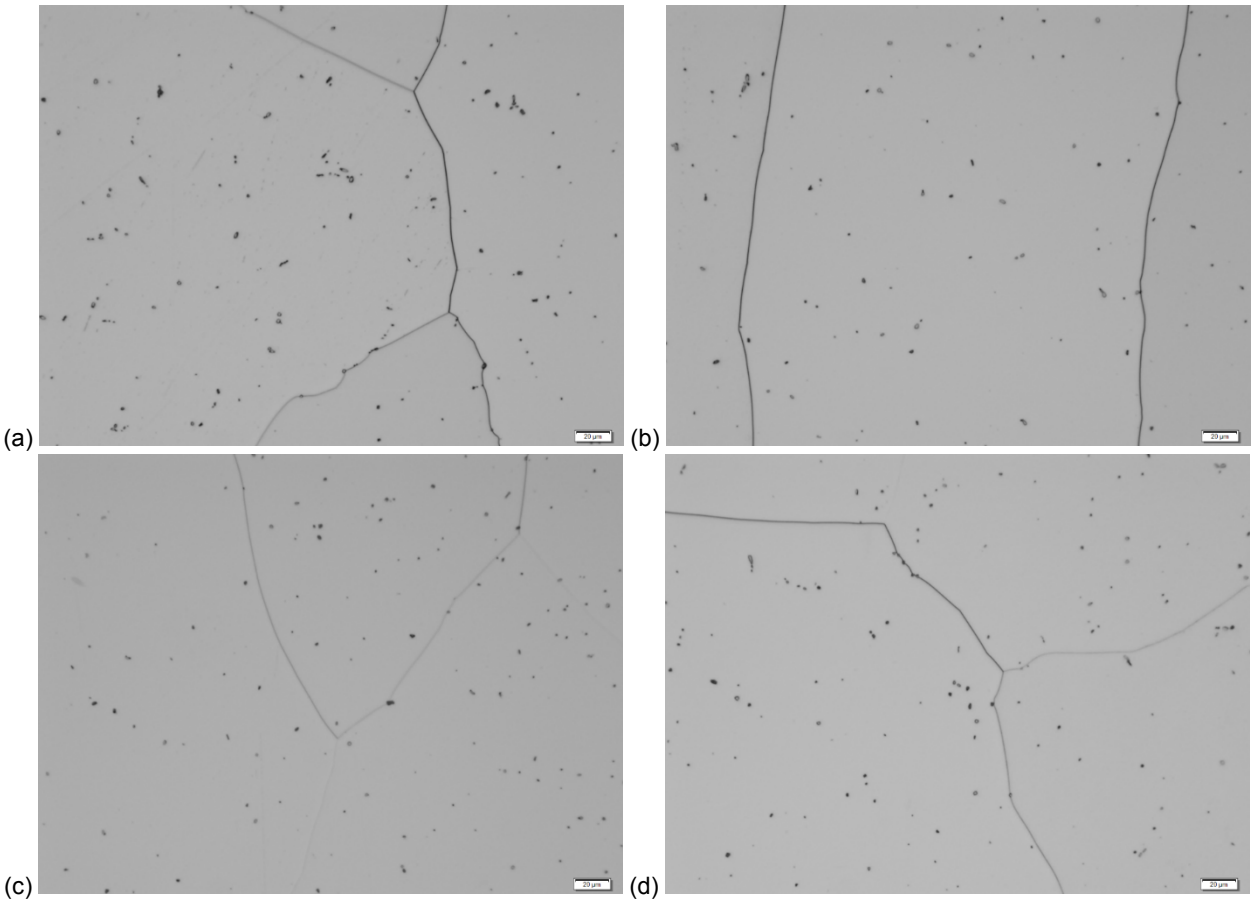

Figure 30.—Photomicrographs showing alloys (a) 52-5H, (b) 53-5H, (c) 54-5H, and (d) 55-5H after heat treatment at 1,000 °C. These photomicrographs show that essentially no precipitation products are formed in these alloys during this heat treatment.

Second Phase

Figures 31 through 34 show the average second phase volume percent for the studied compounds.

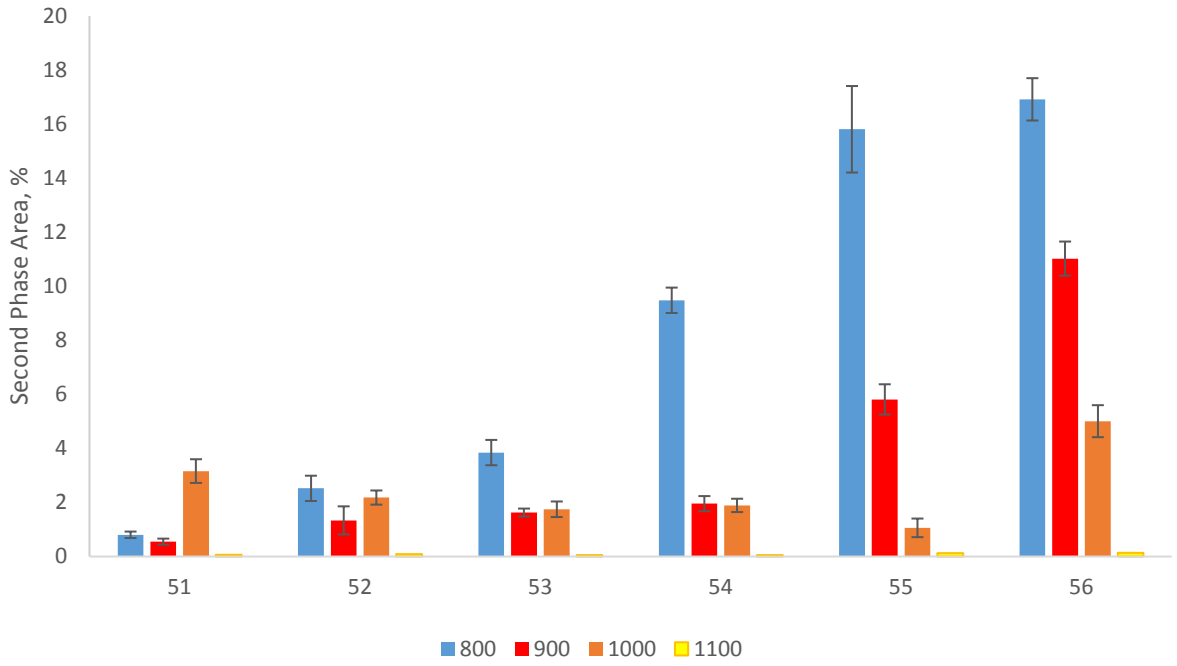

Figure 31.—Second phase area percent for binary alloys 51 through 56.

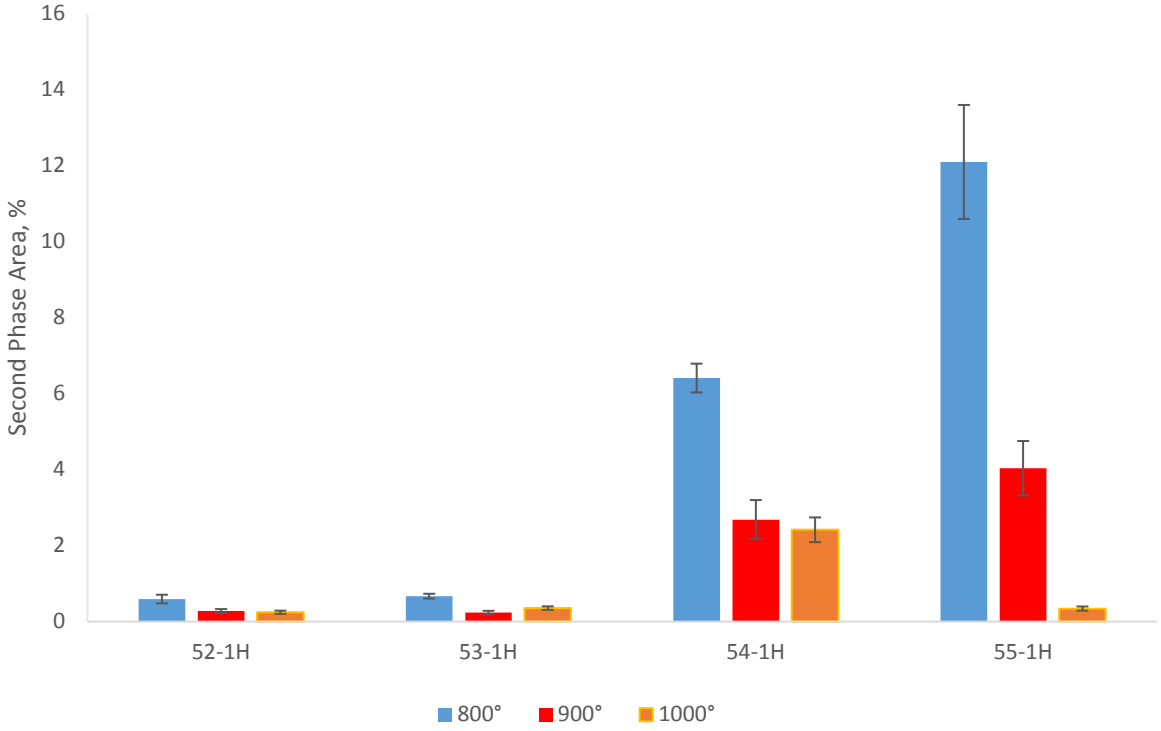

Figure 32.—Second phase area percent for alloys containing 1 at.% Hf.

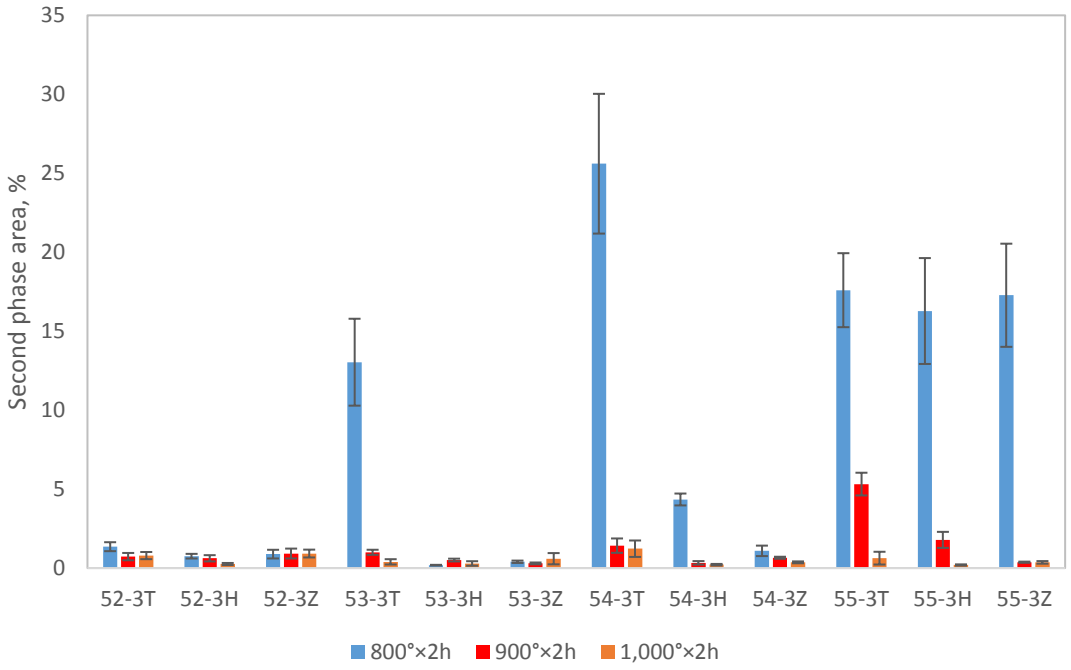

Figure 33.—Second phase area percent for Ni-Ti-3X alloys, where X is Ta, Hf or Zr.

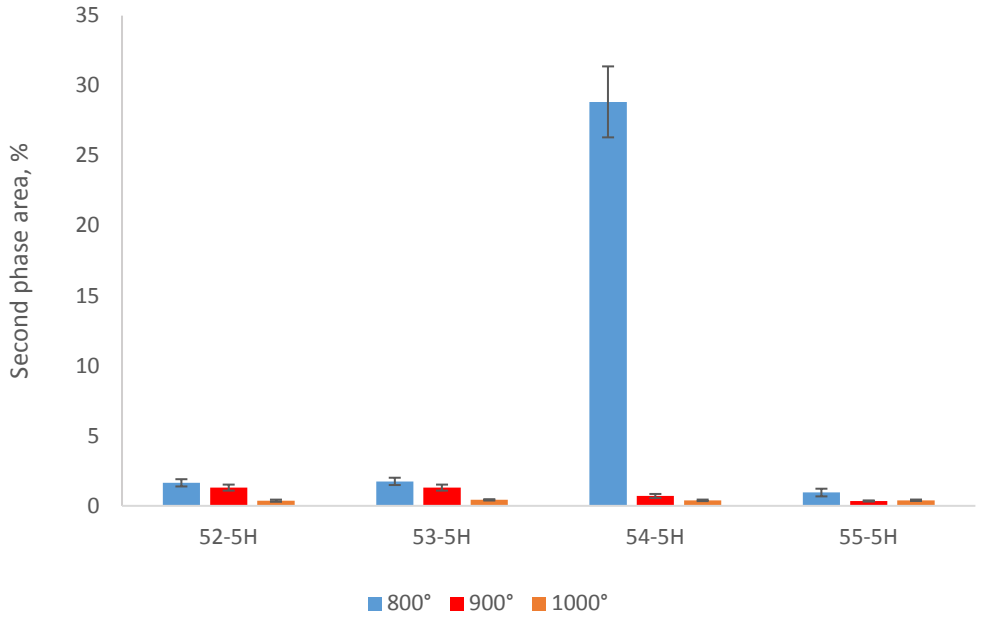

Figure 34.—Second phase area percent for alloys containing 5 at.% Hf.

Microindentation Hardness

Figures 35 through 38 show the average hardness measurements for each compound.

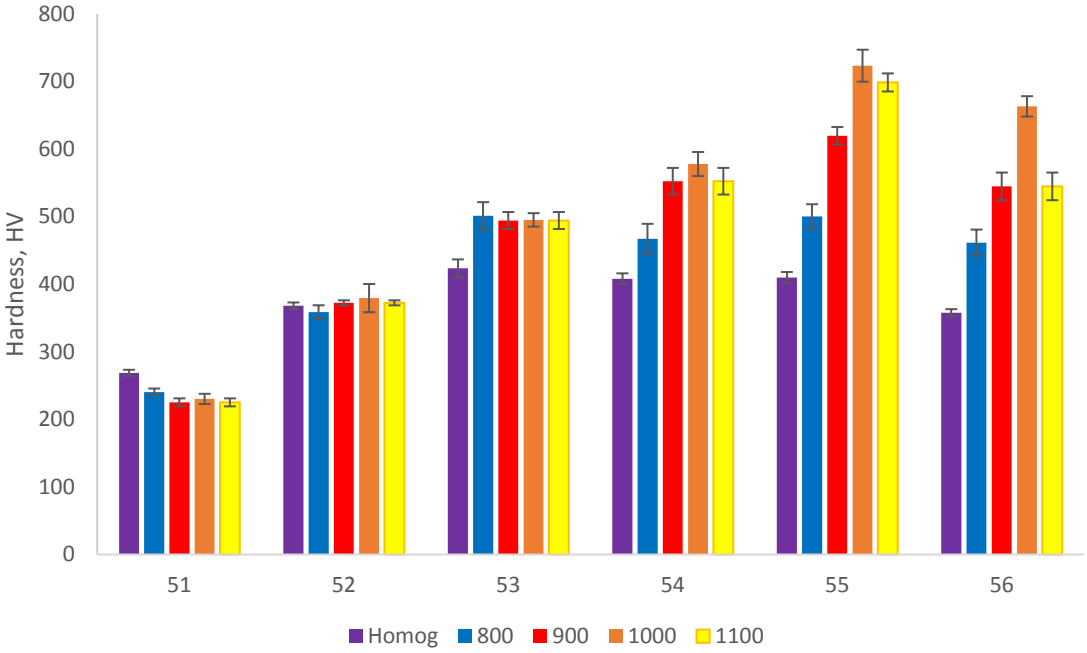

Figure 35.—Hardness for the binary Ni-Ti alloys in this study.

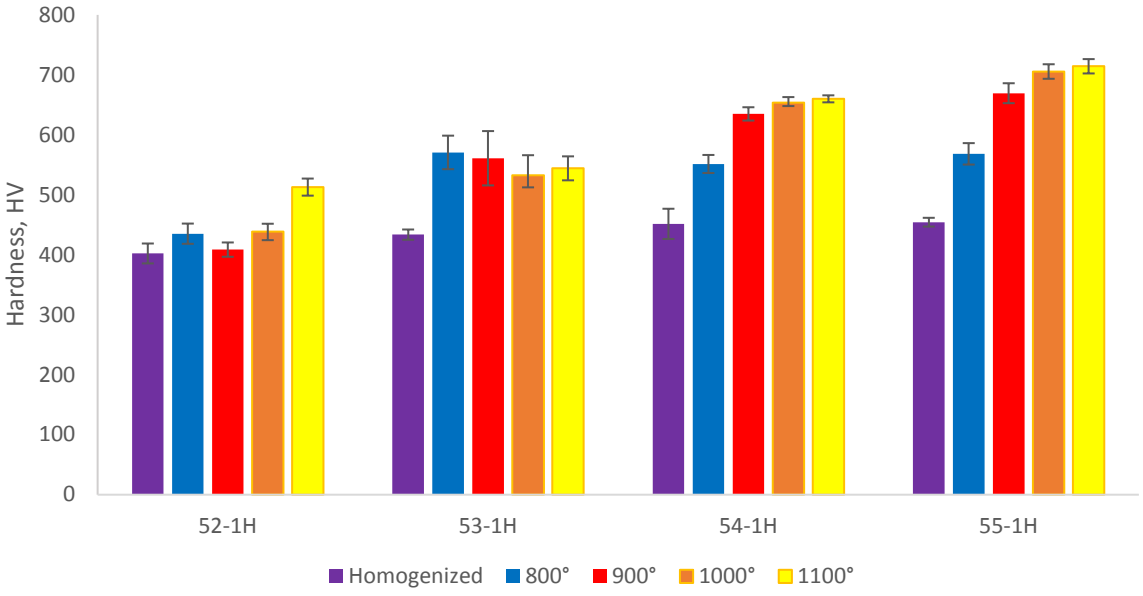

Figure 36.—Hardness for ternary alloys containing 1 at.% Hf.

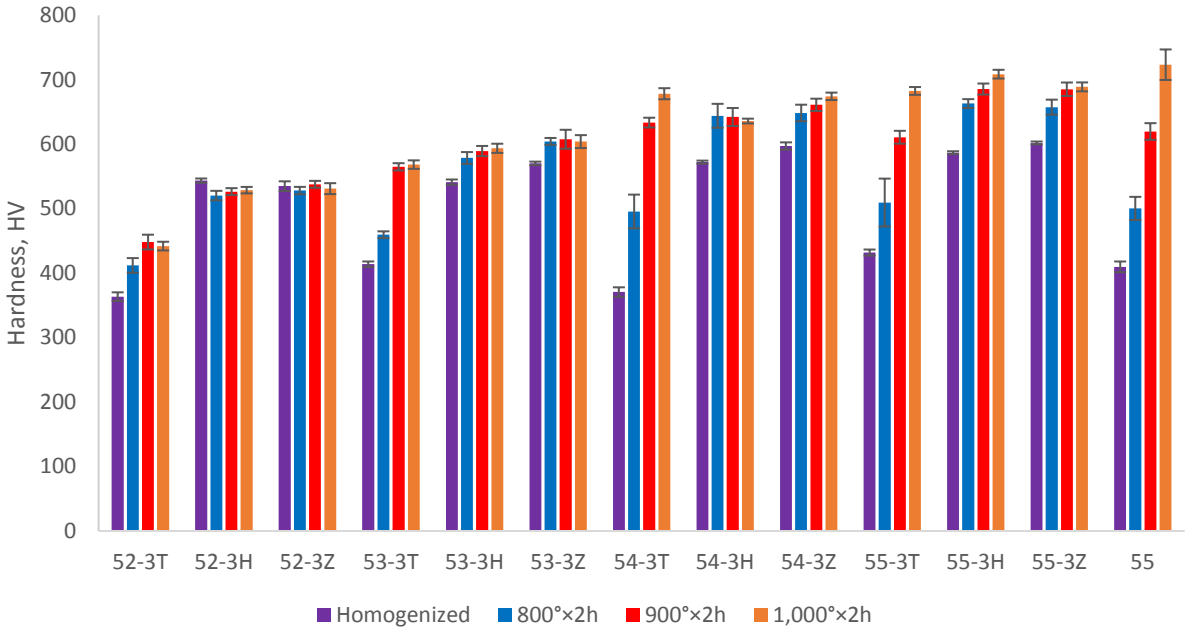

Figure 37.—Hardness of the Ni-Ti-X alloys in this study where X is 3 at.% Ta, Hf or Zr.

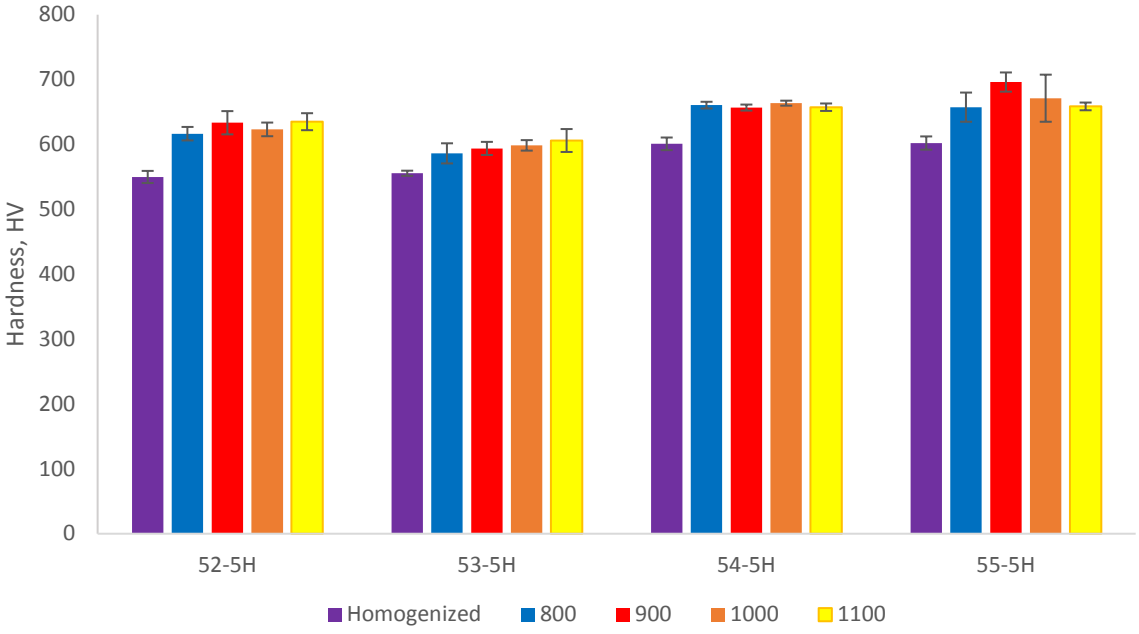

Figure 38.—Hardness of the ternary alloys in this study containing 5 at.% Hf.

Summary Remarks

This report shows that the highest hardness of the studied binary Ni-Ti compounds was achieved with alloy 55 (55 at.% Ni – 45 at.% Ti), after heat treatment at 1,000 °C. This heat treatment is severe and has been found to result in warping and quench cracking. After heat treatment at a less severe temperature of 900 °C, alloy 55 had a hardness of approximately 620 HV. This hardness was exceeded when alloys 54-1H, 55-1H, 54-3T, 54-3H, 54-3Z, 55-3H, 55-3Z, 52-5H, 54-5H, and 55-5H, were heat treated at 900 °C or higher and for alloys 54-3H, 54-3Z, 55-3H, 55-3Z, 54-5H, and 55-5H even when they were heat treated as low as 800 °C. The heat treatments rendered these alloys with less than approximately 3 percent secondary phase area fraction, indicating that the microstructures were essentially free of secondary phase precipitates (with only oxides or carbides remaining) except for alloys 54-3H, 55-3H, 55-3Z, and 54-5H after the 800 °C heat treatment. Incidentally, alloy 55 had a secondary phase area fraction of approximately 6 percent after heat treatment at 900 °C. Secondary phases reduce hardening in the material, as mentioned previously, and likely degrade fatigue strength by serving as crack initiation sites.

This study shows that alloys 54-3Z, 55-3H, 55-3Z, 54-5H and 55-5H had hardness values of approximately 660HV (≈58HRC) or higher after heat treatment at 900 °C. Each of these alloys had microstructures with negligible secondary phase area fractions. This information should be useful to designers interested in the development of applications employing superelastic, hard, corrosion-resistant materials such as gears and bearings.

References

1. W.J. Buehler and F.E. Wang, "A Summary of Recent Research on Nitinol Alloys and Their Potential Application in Ocean Engineering," *Ocean Engineering*, Vol. 1, pp. 105–20, 1968.
2. C. DellaCorte, S.V. Pepper, R.D. Noebe, D.R. Hull and G. Glennon, Intermetallic Nickel-Titanium Alloys for Oil-Lubrication Bearing Applications, NASA/TM—2009-215646, March 2009.
3. S.V. Pepper, C. DellaCorte, R.D. Noebe, D.R. Hull and G. Glennon, Nitinol 60 as a Material for Spacecraft Triboelements, ESMATS 13 Conference, Vienna, Austria, September 2009.
4. C. DellaCorte, R.D. Noebe, M.K. Stanford, S.A. Padula, "Resilient and Corrosion-Proof Rolling Element Bearings Made From Superelastic Ni-Ti Alloys for Aerospace Mechanism Applications," NASA/TM—2011-217105, NASA Center for Aerospace Information, Hanover, MD, 2011.
5. D.M. Poole and W. Hume-Rothery, "The Equilibrium Diagram of the System Nickel-Titanium," Journal of the Institute of Metals, Vol. 83, pp. 473–79, 1954–55.
6. B.C. Hornbuckle, R.D. Noebe and G.B. Thompson, Influence of Hf Solute Additions on the Precipitation and Hardenability in Ni-rich NiTi Alloys, Journal of Alloys and Compounds, Vol. 640, pp. 449–54, 2015.
7. B.C. Hornbuckle, Investigation in Phase Stability and Mechanical Attributes in Very Ni-rich Nitinol With and Without Hafnium Additions, Ph.D. dissertation, University of Alabama, August 2014.
8. W.H. Wilson and R.W. Staehle, "History of Hafnium," in The Metallurgy of Hafnium, Naval Reactors, Division of Reactor Development, United States Atomic Energy Commission, D.E. Thomas and E.T. Hayes eds., U.S. Government Printing Office, Washington, DC, 1960.
9. G.L. Miller, "Zirconium," 2nd ed., Academic Press Inc., New York, 1957.
10. Choudhury, Vacuum Metallurgy, ASM International, Materials Park, OH, 1990.
11. R.R. Adharapurapu, F. Jiang and K.S. Vecchio, "Aging Effects on Hardness and Dynamic Compressive Behavior of Ti-55Ni (at.%) Alloy," Materials Science & Engineering A, vol. 527, pp. 1665–76, 2010.
12. M. Nishida, C.M. Wayman and T. Honma, "Precipitation Processes in Near-Equiatomic TiNi Shape Memory Alloys," Metallurgical Transactions A, Vol. 17A, 1986, pp. 1505–1515.
13. ASTM Designation E 384-11$^{\varepsilon 1}$, "Standard Test Method for Knoop and Vickers Hardness of Materials," 2011, Vol. 03.01, American Society for Testing and Materials, West Conshokocken, PA.